


# 國立交通大學

電信工程學系

碩士論文



利用外來資訊轉換圖設計第一類混合自動重傳之位元對應在位元交錯調變碼之迭代解碼系統

EXIT-Chart Based Labeling Design for Type-I  
HARQ in BICM-ID Systems

研究生：蔡文傑

指導教授：沈文和 教授

中華民國九十六年九月

利用外來資訊轉換圖設計第一類混合自動重傳之位元對應在  
位元交錯調變碼之迭代解碼系統

EXIT-Chart Based Labeling Design for Type-I  
HARQ in BICM-ID Systems

研 究 生：蔡文傑

Student：Wen-Chieh Tsai

指 導 教 授：沈文和

Advisor：Dr. Wern-Ho Sheen



Submitted to Institute of Communication Engineering  
College of Electrical Engineering and Computer Science

National Chiao Tung University

in partial Fulfillment of the Requirements

for the Degree of

Master of Science

in

Communication Engineering

September 2007

Hsinchu, Taiwan, Republic of China

中華民國九十六年九月

# 利用外來資訊轉換圖設計第一類混合自動重傳之位元對應在 位元交錯調變碼之迭代解碼系統

學生：蔡文傑

指導教授：沈文和 博士

國立交通大學電信工程學系（研究所）碩士班

## 摘 要

在現代的無線通訊系統中，位元交錯調變碼被利用來克服瑞雷（Rayleigh）衰減通道，而混和自動重傳機制則可用來提升系統的吞吐量，兩者均是下一代通訊系統所採用的重要技術。在本論文中，我們針對第一類混和自動重傳機制（Type-I Hybrid Auto-retransmission Request）在位元交錯調變碼之迭代解碼（BICM-ID）系統架構下提出一個位元對應（Labeling）及解碼器（Decoder）設計的方法。利用外來資訊轉換圖（EXIT Chart）這個強大的工具，我們提出一個可根據外部錯誤更正碼來設計重傳時所用位元對應的演算法。根據所找出的位元對應，我們利用鏈路調節（Link adaptation）的概念在不同的通道訊雜比（SNR）下使用不同的位元對應來得到較佳的品質。最後，我們根據 3GPP 的渦輪碼（Turbo Code）提出一個新穎的解碼器設計，結合適當的位元對應具有優於現今 3GPP 規範裡設計的品質

# EXIT-Chart Based Labeling Design for Type-I HARQ in BICM-ID Systems

Student : Wen-Chieh Tsai  
Sheen

Advisors : Dr. Wern-Ho

Department of Communication Engineering  
National Chiao Tung University

## ABSTRACT

In modern wireless communication systems, bit-interleaved coded modulation (BICM) is used to overcome the Rayleigh fading channel, and the HARQ (Hybrid Auto-retransmission Request) technique is used to improve the system throughput. In this thesis, we propose new labeling and decoder designs for Type-I HARQ for BICM-ID systems. Based on the EXIT (Extrinsic Information Transfer) chart, we develop an algorithm to search for good labeling for retransmission that well matches with the outer code. The concept of link adaptation is realized by using different labeling at different SNR (signal to noise ratio) to achieve a better performance. Finally, a novel decoding strategy is proposed along with the proposed labeling design for turbo code in 3GPP specification. It is shown that the new design outperforms the existing one.

## 致謝

本篇論文得以完成首先要感謝我的指導教授 沈文和博士，在兩年做研究過程中，給予我非常多而且重要的指導，得以研究解決有意義的問題，並使我了解研究做學問所該具有的謹慎態度；另外，要感謝王忠炫教授，在每星期的集會中給予我許多受用的建議及做研究的方向；也要感謝口試委員陳仁智博士的指正與建議，讓本論文更加完善。

在此也要感謝實驗室的同学學長們，時常與我共同討論論文上遇到的問題，在許多次反覆的討論下，得以找出解決問題的最好方法，讓論文得以順利完成。



最後要感謝我的家人，在這兩年的過程中不斷的鼓勵我支持我，讓我生活無憂無慮得以專心做研究，遇到問題也可以讓我有休息的機會，好好整理心情再出發，無論遇到如何的挫折都會陪我一起度過難關，謝謝你們。

民國九十六年九月

研究生蔡文傑謹致於交通大學

# Contents

摘要

Abstract

致謝

Lists of Tables

Lists of Figures

**Chapter 1 : Introduction ..... 1**

**Chapter 2 : Basic Concep..... 4**

2.1 Hybrid ARQ ( HARQ ) [12] .....4

2.1.1 Type-I HARQ .....5

2.1.2 Type-II HARQ .....6

2.1.3 Type-III HARQ .....6

2.2 Throughput in HARQ system .....7

**Chapter 3 : System Model ..... 9**

3.1 System Model of HARQ in BICM-ID .....9

3.1.1 Bit Level Inter-leaver .....9

3.1.2 Modulator .....10

3.2 Iterative Decoding .....11

3.2.1 Detector .....11

3.2.2 Decoder .....13

**Chapter 4 : Extrinsic Information Transfer Curve ( EXIT ) Chart**

**.....18**

4.1.1 : Transfer Characteristic .....18

4.1.2 : Transfer Curve of Decoder .....21

4.1.3 : Transfer Curve of Detector .....22

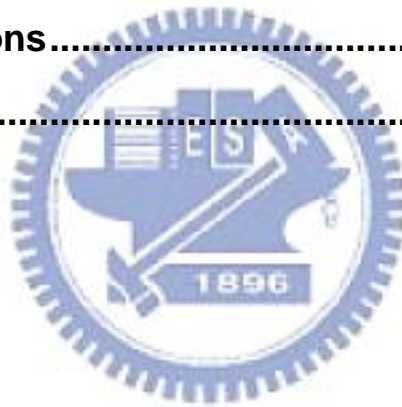
4.1.4 : EXIT Chart .....26

**Chapter 5 : The Proposed Searching Algorithm.....29**

5.1 Simplified Model .....29

5.1.1 Hard Decision Virtual Channel .....29

5.1.2 Binary Symmetric Extrinsic Channel.....	32
5.1.3 Closed-form EXIT function .....	33
5.2 Searching Algorithm .....	36
5.3 Simulation Results .....	40
5.3.1 CC ( 133 <sub>8</sub> ,171 <sub>8</sub> ) , 16QAM, Rayleigh channel.....	40
5.3.2 CC ( 133 <sub>8</sub> ,171 <sub>8</sub> ) , 8PSK, Rayleigh channel.....	45
<b>Chapter 6 : Design for 3GPP Turbo Code.....</b>	<b>48</b>
6.1 HARQ in 3GPP for Turbo Code .....	48
6.2 Labeling Design for Turbo Code .....	50
6.3 Novel Decoder Design for Turbo Code .....	53
6.4 Analysis of Conventional and Modified Decoder.....	54
6.4.1 Information theoretical point of view .....	54
6.4.2 Numeric Values .....	56
6.5 Simulation Results .....	58
<b>Chapter 7 : Conclusions.....</b>	<b>61</b>
<b>Reference.....</b>	<b>62</b>



## List of Tables

Table 5.1 Table used for searching algorithm.....	38
Table 5.2. Simulation parameter of CC ( $133_8$ , $171_8$ ) .....	40
Table 5.3 Strategy of link adaptation for CC ( $133_8$ , $171_8$ ) with 16-QAM .....	41
Table 5.4 Strategy of link adaptation for CC ( $133_8$ , $171_8$ ) with 8-PSK .....	45
Table 6.1 Mapping functions for constellation rearrangement .....	50
Table 6.2 Mapping functions for our design, (a) candidates for second transmission and the optimal one, (b) candidate for third transmission and the optimal one .....	51
Table 6.3 Analysis in information theoretically point of view for conventional scheme and modified scheme .....	55
Table 6.4 Simulation parameter for 3GPP turbo code.....	56





## List of Figures

Fig. 2.1 Block diagram of Type-I HARQ .....	5
Fig. 2.2 Block diagram of Type-II HARQ.....	6
Fig. 2.3 Block diagram of Type-III HARQ .....	7
Fig. 3.1 BICM with Type-I HARQ System Model.....	9
Fig. 3.2 16QAM and 8-PSK constellations and the corresponding Gray labeling.....	10
Fig. 3.3 BICM-ID System Model.....	11
Fig. 4.1 Soft-input-soft-output (SISO) decoder (a) and detector (b) .....	19
Fig. 4.2 the relation between $I_A$ and $\sigma_A$ .....	20
Fig. 4.3 Transfer curves of several convolutional code with distinct constrain length and of 3GPP turbo code.....	22
Fig. 4.4 Block diagram of detector (demapper) .....	22
Fig. 4.5 Transfer curves of several labeling in AWGN and Rayleigh fading channel.....	25
Fig. 4.6 Transfer curves of Gray labeling under distinct channel condition (SNR) .....	26
Fig. 4.7 Example of trajectory under iterative decoding .....	28
Fig. 4.8 Transfer curves of distinct labeling under identical channel condition (SNR) .....	28
Fig. 5.1 Capacity for real communication channel and virtual channel (AWGN) .....	32
Fig. 5.2 Capacity for real communication channel and virtual channel (Rayleigh) ...	32
Fig. 5.3 Binary Symmetric Extrinsic Model.....	33
Fig. 5.4 Two transmissions for 16QAM under Rayleigh fading channel.....	35
Fig. 5.5 Three transmissions for 16QAM under Rayleigh fading channel.....	35
Fig. 5.6 Transfer curves of several labeling pair with fixed 1st mapping function .....	37
Fig. 5.7 Transfer curves of the suitable labeling in our design for CC (133 <sub>8</sub> , 171 <sub>8</sub> ) with 16-QAM.....	42
Fig. 5.8 Throughput and PER of the suitable labeling for CC (133 <sub>8</sub> , 171 <sub>8</sub> ) with 16-QAM under T = 2.....	43
Fig. 5.9 Throughput of the suitable labeling for CC (1338, 1718) with 16-QAM under T = 3 .....	44
Fig. 5.10 Throughput and PER of the suitable labeling for CC (133 <sub>8</sub> , 171 <sub>8</sub> ) with 8-PSK under T = 2.....	46
Fig. 5.11 Throughput and PER of the suitable labeling for CC (133 <sub>8</sub> , 171 <sub>8</sub> ) with 8-PSK with 8-PSK under T = 3 .....	47
Fig. 6.1 Transfer curves of labeling of chase combining and constellation rearrangement. .....	49
Fig. 6.2 Transfer curves of labeling of chase combining and our design. ....	52
Fig. 6.3 System model of BICM-ID with turbo code .....	53
Fig. 6.4 System model of BICM-ID with turbo code .....	55
Fig. 6.5 Mutual information between information bit and 1 <sup>st</sup> decoder extrinsic .....	57
Fig. 6.6 Mutual information between information bit and 2 <sup>nd</sup> decoder extrinsic .....	57

Fig. 6.7 Trajectory of iterative decoding in our design.....58  
Fig. 6.8 BER of constellation rearrangement (□) and our design (○) .....59  
Fig. 6.9 PER of constellation rearrangement (□) and our design (○) .....60  
Fig. 6.10 Throughput of constellation rearrangement (□) and our design (○) .....60



## Chapter 1 : Introduction

Since 1982, when Ungerboeck proposed trellis-coded modulation (TCM) mainly for AWGN channels [1], it has been generally accepted that coding and modulation should be jointly designed for a better system performance. A symbol inter-leaver is applied to increase diversity order to the minimum number of distinct symbols between two code-words. However, when the channel is Rayleigh faded, the code performance depends strongly on its minimum Hamming distance (code diversity) rather than the minimum Euclidean distance of the code [2]. Zehavi proposed a coding modulation scheme, called BICM (Bit-Interleaved Coded Modulation), to increase the code diversity by introducing a bit inter-leaver between encoder and modulator [3]. In [4], the author discovered that using iterative decoding with well-designed labeling the performance of BICM can be improved dramatically. Up to now, BICM has been extensively employed in practical wireless communication systems, such as HSDPA [5] and WiMAX [6].

Hybrid ARQ (Auto-retransmission Request) [4] is another important technique in modern wireless communication systems. It combines the property of forward error control coding (FEC) and ARQ. Roughly speaking, there are three types of HARQ schemes, including chase combining (Type-I) [7], full incremental redundancy (Type-II) [8] and partial incremental redundancy (Type-III). HARQ provides high system reliability, and thus system throughput can be enhanced substantially. HSDPA and WiMAX both employ this technique to attain good performance. Furthermore, HSDPA also utilizes different labeling in HARQ for

retransmissions to gain additional performance enhancement.

EXIT chart proposed by Brink [9] is a powerful tool to analyze convergence behavior of iterative decoding. It uses mutual information between extrinsic output and the corresponding bits to predict the performance of iterative decoding system precisely. Frequently, EXIT chart is used to design turbo code, LDPC code and BICM-ID systems.

In this thesis, EXIT chart is employed to design HARQ for BICM-ID systems. In particular, new labeling that well matches the outer code is design to improve performance. Using labeling obtained in [10] for the first transmission, an algorithm is proposed to search for good labeling for the subsequent transmissions. Link adaptation is realized by using different labeling at different SNR to further improve the performance. In addition, a new decoding method along with new labeling is proposed for the Type-I ARQ with the 3GPP turbo codes. Numerical results shoe that 0.3-0.4 dB improvement is achieved at a sight expense of decoding complexity.

The rests of the thesis is organized as follow. In Chapter 2, we introduce the concept of HARQ and discuss the important parameters to evaluate its performance, In Chapter 3, a system model for HARQ with different labeling for retransmission in BICM-ID system is introduced. In Chapter 4, we explain the EXIT chart of detector and decoder in detail. In Chapter 5, a simplified model for EXIT chart and a searching algorithm are proposed, and a number of simulation results are given for various coding and modulation schemes. In chapter 6, we compare our design with the existing retransmission scheme in 3GPP

specification, and conclusions are given in Chapter 8.



## Chapter 2 : Basic Concep

### 2.1 Hybrid ARQ ( HARQ ) [12]

Forward Error Control (FEC) and Auto-retransmission Request (ARQ) schemes are two techniques for controlling transmission error in data transmission systems. In a FEC system, a good error-correcting code is used. While the receiver detects the presence of errors in a received packet, it attempts to determine the error locations and then corrects those errors. After decoding, the receiver accepts the packet no matter it is error-free or erroneous. In an ARQ system, a code with good error-detecting capability is used. If the received packet is detected as error-free, it will be accepted by the receiver. At the same time, the receiver sends a positive acknowledgment (ACK) to transmitter via a return channel to notify that the packet has been successfully received. If the received packet is detected as erroneous, the receiver send a negative acknowledgment (NACK) to transmitter and request transmitter to retransmit the same packet. Retransmission continues until either that the packet is successfully received or that errors repeatedly occur to the maximum retransmission number for that packet.

Comparing FEC with ARQ, we see that ARQ is simple and provides high system reliability, however, throughput of ARQ falls rapidly with increasing channel error rate. FEC keeps higher throughput than ARQ, but it is hard to achieve high system reliability because the probability of decoding error is much greater than probability of an undetected error.

FEC and ARQ can be combined properly to exploit respective advantages and overcome drawbacks. Such a combination of the two schemes is referred to as a hybrid ARQ.

### 2.1.1 Type-I HARQ

As shown in Fig.2.1, In the Type-I HARQ scheme if the receiver fails to decode the transmitted coded packet, a retransmission request, NACK, is fed back from receiver to transmitter. Upon reception of this NACK, the transmitter sends the same coded packet again. The receiver needs to buffer all previously received packets and combine those with recently received packet according to maximal ratio combining (MRC), which was first discussed by Chase [7]. Hence, the Type-I HARQ is also referred to as "Chase Combining" (CC).

Type-I HARQ provides diversity gain by decoding a packet because of combining multiple received signals. To perform Type-I HARQ, it needs only an additional buffer to save received packets compared with the conventional ARQ, but the feedback and decoding schemes are the same as those in the conventional ARQ.

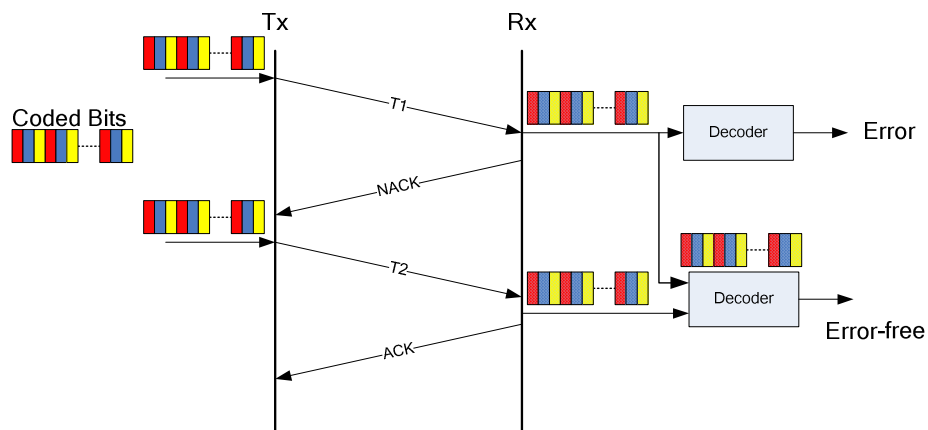


Fig. 2.1 Block diagram of Type-I HARQ

## 2.1.2 Type-II HARQ

In real communication systems, coded bits coming out from encoder need to be punctured before transmission in order to improve the bandwidth efficiency. Type-II HARQ utilizes the property of punctured code. As in Fig. 2.2, the coded bits are punctured to three parts A, B and C. At the first transmission, transmitter sends punctured coded bits A and B to receiver for example. If the receiver fails to decode the packet, the transmitter sends additional coded bits, that is, the redundant bits C. Instead of sending the same coded packet, the transmitter sends additional coded parts, when a NACK is received.

Type-II HARQ provides an extra coding gain for decoding a packet since the receiver combines received packets to form as a low rate code. With the property of retransmitting different coded bits, Type-II HARQ is called “Incremental Redundancy” (IR).

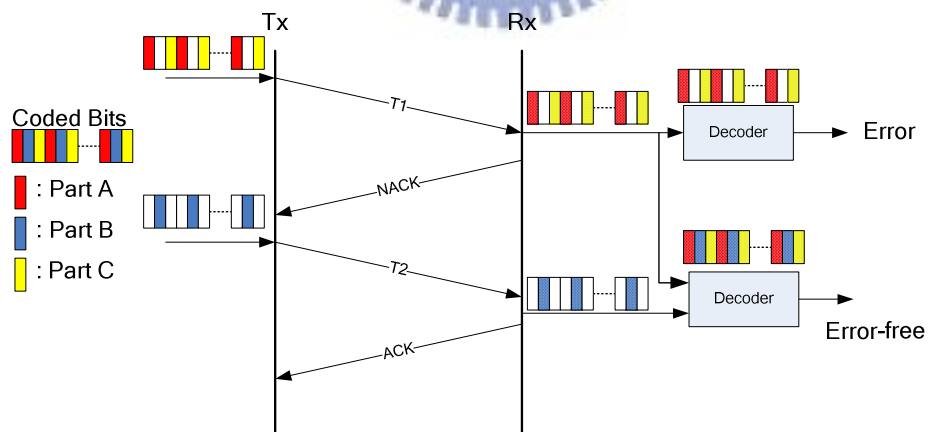


Fig. 2.2 Block diagram of Type-II HARQ

## 2.1.3 Type-III HARQ

In Type-III HARQ, each retransmission is self-decodable and is composed of not



only redundant bits but identical bits. The identical bits are combined using MRC, and the redundant bits are exploited to form a lower rate code with stronger error correction capability. Type-III HARQ inherits the advantages of Type-I and Type-II HARQ and is called “Partial Incremental Redundancy”. Fig. 2.3 shows the block diagram of Type-III HARQ.

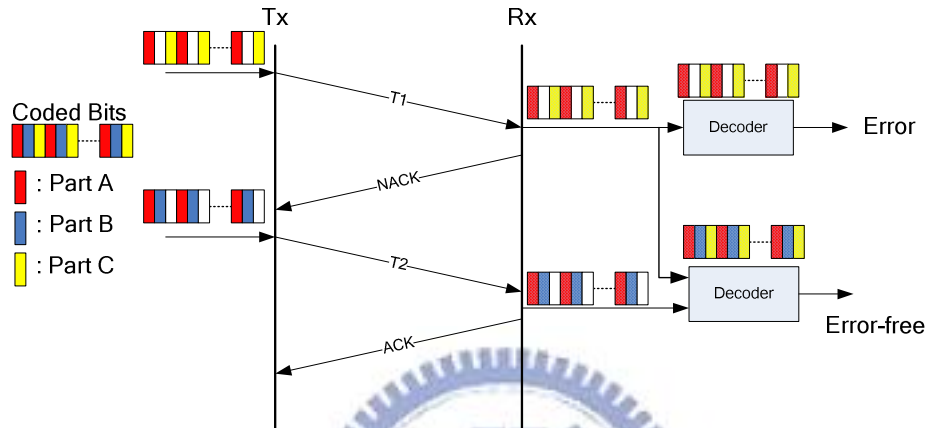


Fig. 2.3 Block diagram of Type-III HARQ

## 2.2 Throughput in HARQ system

A key performance metric for HARQ is its throughput, which is the number of bits conveyed per unit time. In a type-I HARQ system, the information we want to deliver are encoded as binary coded bits sequence, namely, data packet. During the HARQ process, a data packet can be sent to the receiver using  $M$  transmission packets at most, that is  $M$  is the maximum transmission number for a data packet. Suppose modulation scheme is identical during retransmission, the throughput of type-I HARQ can be calculated as follow. Assume  $N$  is the number of data packets sent to the receiver. The throughput is given by

$$\begin{aligned} \text{Throughput}(\text{bits/sec}) &= \frac{\# \text{ of successfully received information bits}}{\text{Time to deliver } N \text{ data packets}} \\ &= \frac{\# \text{ of successfully received data packet} * r}{\# \text{ of transmitted transmission packet} * R} \end{aligned}$$

where  $r$  is the code rate, and  $R$  is the packet transmission rate. Since  $r$  and  $R$  are fixed, we define another metric  $\Psi$  in place of throughput for convenience.

$$\Psi = \frac{\# \text{ of successfully received data packet}}{\# \text{ of transmitted transmission packet}}, \quad 0 \leq \Psi \leq 1$$



## Chapter 3 : System Model

### 3.1 System Model of HARQ in BICM-ID

Fig.3-1 shows the system model of BICM with Type-I HARQ. A binary information data  $\mathbf{b}$  is encoded as codeword  $\mathbf{c}$ , and a bit level inter-leaver  $\Pi$  located between encoder and modulator converts  $\mathbf{c}$  to a bit sequence  $\mathbf{c}'$ . The modulation scheme has an  $M$ -ary constellation signal set  $\mathcal{X} = \{x_1, \dots, x_M\}$  with  $M = 2^m$ .  $\mathbf{c}'$  is put into modulator sequentially and every  $m$  bits are grouped to form a label  $\mathbf{s} = [c_0, \dots, c_{m-1}]$ . Let  $\Lambda$  be the set of all possible labels,  $|\Lambda| = 2^m$ . Through the modulator, a constellation point  $x = \mu(\mathbf{s})$  is selected according to a labeling mapping function  $\mu$ .  $\mu_i$  represents the mapping function used in  $i$ -th transmission.

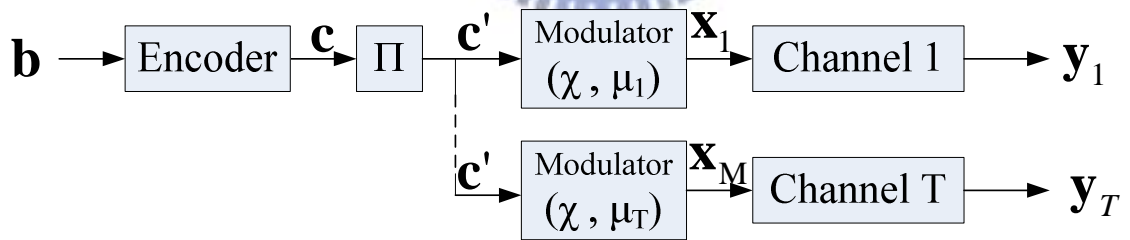


Fig. 3.1 BICM with Type-I HARQ System Model

#### 3.1.1 Bit Level Inter-leaver

The inter-leaver used in the system is S-random inter-leaver [13]. An S-random interleaver guarantees that the two bits within a distance  $S_1$  at the interleaver input can not be mapped to a distance less than  $S_2$  apart at the interleaver output. Usually  $S_1 = S_2 = S$ .

Define an interleaving function  $\pi : c_j = c'_{\pi(j)}$ . If

$$|i - j| < S \quad (3-1)$$

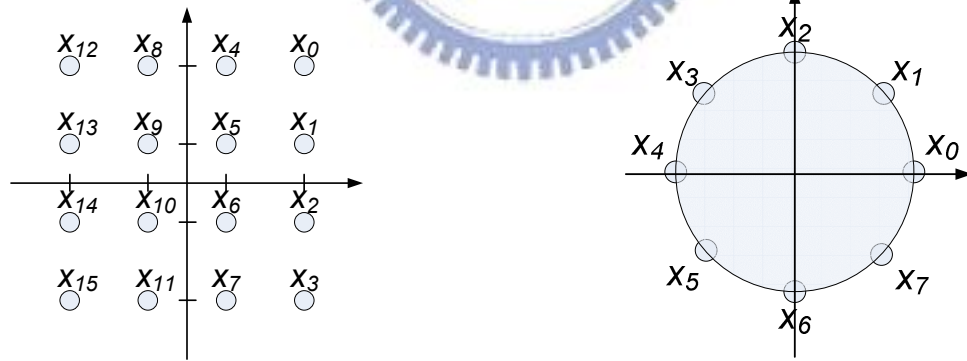
Then the design guarantees that

$$|\pi(i) - \pi(j)| > S \quad (3-2)$$

### 3.1.2 Modulator

The coded bits coming out from encoder followed by bit inter-leaver are grouped every  $m$  bits and mapped to constellation point by specific mapping function. In the thesis, we consider only 16-QAM and 8PSK constellations as shown Fig. 3.2.

The mapping function maps a transmitted label to a constellation point, for instance, a Gray mapping function for 16QAM and 8PSK are shown in Fig. 3.2.



$\mu_{Gray,16QAM}(s)$	$x_0$	$x_1$	$x_2$	$x_3$	$x_4$	$x_5$	$x_6$	$x_7$	$x_8$	$x_9$	$x_{10}$	$x_{11}$	$x_{12}$	$x_{13}$	$x_{14}$	$x_{15}$
$s$	3	2	6	7	1	0	4	5	9	8	12	13	11	10	14	15

$\mu_{Gray,8PSK}(s)$	$x_0$	$x_1$	$x_2$	$x_3$	$x_4$	$x_5$	$x_6$	$x_7$
$s$	0	5	2	7	4	1	6	3

Fig. 3.2 16QAM and 8-PSK constellations and the corresponding Gray labeling

## 3.2 Iterative Decoding

Since the optimal decoding strategy for BICM system, that is, MAP, is too complex to implement, we separate the receiver into two parts : detector and decoder. And the detector and the decoder exchange soft information iteratively.

Fig. 3.3 shows a diagram of iterative decoding for BICM HARQ. The detector  $\phi$  takes channel outputs  $\mathbf{y}_1, \dots, \mathbf{y}_M$ , and intrinsic LLRs from decoder,  $\mathbf{L}_A^{(\phi)}$ , to compute extrinsic LLRs,  $\mathbf{L}_E^{(\phi)}$ . Then, the extrinsic LLRs of detector are de-interleaved and serve as a priori inputs  $\mathbf{L}_A^{(\phi)}$  of decoder.

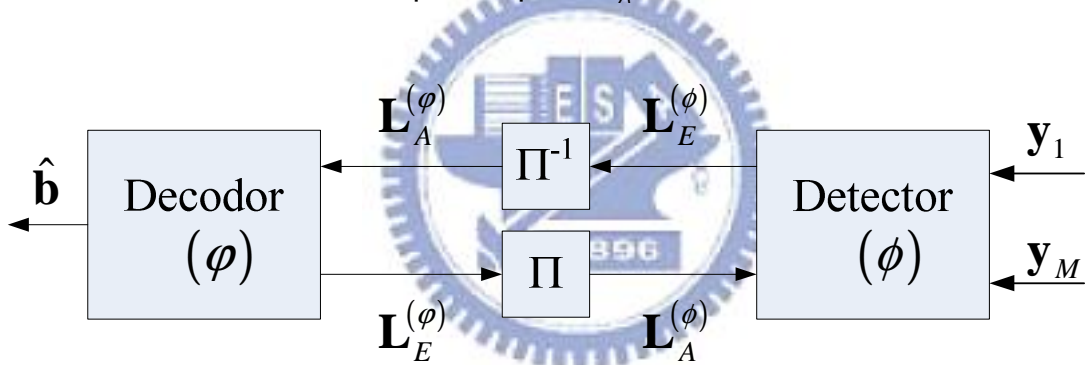


Fig. 3.3 BICM-ID System Model

### 3.2.1 Detector

The APP detector is used to compute the a posteriori probability for coded bits. Since memory-less modulation scheme is used, we demodulate received signal symbol by symbol. The APP for bit  $c_i$  in a symbol,  $L_D^{(\phi)}(i)$  is

$$\begin{aligned}
L_D^{(\phi)}(i) &= \log \frac{\Pr(c_i = 1 | y_1, \dots, y_T)}{\Pr(c_i = 0 | y_1, \dots, y_T)} \\
&= \log \frac{\Pr(c_i = 1)}{\Pr(c_i = 0)} + \log \frac{\Pr(y_1, \dots, y_T | c_i = 1)}{\Pr(y_1, \dots, y_T | c_i = 0)} \\
&= L_A^{(\phi)}(i) + \log \frac{\sum_{s \in \Lambda_i^1} \Pr(y_1, \dots, y_T | c_i = 1, s) \Pr(s | c_i = 1)}{\sum_{s \in \Lambda_i^0} \Pr(y_1, \dots, y_T | c_i = 1, s) \Pr(s | c_i = 0)} \\
&= L_A^{(\phi)}(i) + \log \frac{\sum_{s \in \Lambda_i^1} \Pr(s | c_i = 1) \Pr(y_1, \dots, y_T | \mu_1(s), \dots, \mu_T(s))}{\sum_{s \in \Lambda_i^0} \Pr(s | c_i = 0) \Pr(y_1, \dots, y_T | \mu_1(s), \dots, \mu_T(s))} \\
&= L_A^{(\phi)}(i) + \log \frac{\sum_{s \in \Lambda_i^1} \exp \left( \sum_{\substack{j=0 \\ j \neq i}}^{m-1} c_j^s L_A^{(\phi)}(j) \right) \exp \left( \frac{\sum_{k=1}^T \|y_k - \hat{h}_k \mu_k(s)\|^2}{\sigma^2} \right)}{\sum_{s \in \Lambda_i^0} \exp \left( \sum_{\substack{j=0 \\ j \neq i}}^{m-1} c_j^s L_A^{(\phi)}(j) \right) \exp \left( \frac{\sum_{k=1}^T \|y_k - \hat{h}_k \mu_k(s)\|^2}{\sigma^2} \right)} \\
&= L_A^{(\phi)}(i) + L_E^{(\phi)}(i) \tag{3-3}
\end{aligned}$$

where  $\Lambda_i^b$  is the set of labels with  $i$ -th bit equal to  $b$ , and  $c_j^s$  is  $j$ -th bit of label  $s$ .

The APP detector can be approximated by the max-log detector in order to reduce decoding complexity. From e.q. (3-3), the max-log detector can be written as

$$\begin{aligned}
L_D^{(\phi)}(i) &= L_A^{(\phi)}(i) + \log \frac{\sum_{s \in \Lambda_i^1} \exp \left( \sum_{\substack{j=0 \\ j \neq i}}^{m-1} c_j^s L_A^{(\phi)}(j) \right) \exp \left( \frac{\sum_{k=1}^T \|y_k - \hat{h}_k \mu_k(s)\|}{\sigma^2} \right)}{\sum_{s \in \Lambda_i^0} \exp \left( \sum_{\substack{j=0 \\ j \neq i}}^{m-1} c_j^s L_A^{(\phi)}(j) \right) \exp \left( \frac{\sum_{k=1}^T \|y_k - \hat{h}_k \mu_k(s)\|}{\sigma^2} \right)} \\
&\approx L_A^{(\phi)}(i) + \log \frac{\max_{s \in \Lambda_i^1} \left\{ \exp \left( \sum_{\substack{j=0 \\ j \neq i}}^{m-1} c_j^s L_A^{(\phi)}(j) \right) \exp \left( \frac{\sum_{k=1}^T \|y_k - \hat{h}_k \mu_k(s)\|}{\sigma^2} \right) \right\}}{\max_{s \in \Lambda_i^0} \left\{ \exp \left( \sum_{\substack{j=0 \\ j \neq i}}^{m-1} c_j^s L_A^{(\phi)}(j) \right) \exp \left( \frac{\sum_{k=1}^T \|y_k - \hat{h}_k \mu_k(s)\|}{\sigma^2} \right) \right\}} \\
&= L_A^{(\phi)}(i) + \max_{s \in \Lambda_i^1} \left\{ \sum_{\substack{j=0 \\ j \neq i}}^{m-1} c_j^s L_A^{(\phi)}(j) + \frac{\sum_{k=1}^T \|y_k - \hat{h}_k \mu_k(s)\|}{\sigma^2} \right\} - \max_{s \in \Lambda_i^0} \left\{ \sum_{\substack{j=0 \\ j \neq i}}^{m-1} c_j^s L_A^{(\phi)}(j) + \frac{\sum_{k=1}^T \|y_k - \hat{h}_k \mu_k(s)\|}{\sigma^2} \right\}
\end{aligned} \tag{3-4}$$

### 3.2.2 Decoder

In the BICM-ID system, a SISO decoder is needed to compute soft information passed to detector. In the thesis, BCJR algorithm [14] is utilized.

The log-APP of coded bit  $c_j$ ,  $L_D^{(\phi)}(c_j)$  is written as

$$L_D^{(\phi)}(c_j) \triangleq \log \frac{\Pr(c_j = 1 | \mathbf{L}_A^{(\phi)})}{\Pr(c_j = 0 | \mathbf{L}_A^{(\phi)})} \tag{3-5}$$

Then, making use of the trellis structure of convolutional code, equation (3-5) can be reformulated as

$$L_D^{(\varphi)}(c_j) = \log \frac{\sum_{(s',s) \in \Sigma_l^1} \Pr(s_l = s', s_{l+1} = s, \mathbf{L}_A^{(\varphi)})}{\sum_{(s',s) \in \Sigma_l^0} \Pr(s_l = s', s_{l+1} = s, \mathbf{L}_A^{(\varphi)})} \quad (3-6)$$

$\Sigma_l^b$  is the set of state pairs that correspond to the coded bit  $c_j = b$  at time  $l$ .

Next we show how the joint probability in (3-6) can be evaluated recursively.

$$\begin{aligned} & \Pr(s_l = s', s_{l+1} = s, \mathbf{L}_A^{(\varphi)}) \\ &= \Pr(s', s, \mathbf{L}_A^{(\varphi)}(t < l), \mathbf{L}_A^{(\varphi)}(t=l), \mathbf{L}_A^{(\varphi)}(t > l)) \\ &= \Pr(\mathbf{L}_A^{(\varphi)}(t > l) | s', s, \mathbf{L}_A^{(\varphi)}(t < l), \mathbf{L}_A^{(\varphi)}(t=l)) \Pr(s, \mathbf{L}_A^{(\varphi)}(t=l) | s', \mathbf{L}_A^{(\varphi)}(t < l)) \Pr(s', \mathbf{L}_A^{(\varphi)}(t < l)) \\ &= \Pr(\mathbf{L}_A^{(\varphi)}(t > l) | s) \Pr(s, \mathbf{L}_A^{(\varphi)}(t=l) | s') \Pr(s', \mathbf{L}_A^{(\varphi)}(t < l)) \end{aligned} \quad (3-7)$$

where  $\mathbf{L}_A^{(\varphi)}(t > l)$  represents the portion of a prior LLRs after time  $l$ , and  $\mathbf{L}_A^{(\varphi)}(t < l)$  the portion of a prior LLRs before after time  $l$ . The last equality follows from the fact that the probability of the state at time  $l$  depends only on the previous states before time  $l$ .

Defining

$$\begin{aligned} \alpha_l(s') &\triangleq \Pr(s', \mathbf{L}_A^{(\varphi)}(t < l)) \\ \gamma_l(s', s) &\triangleq \Pr(s, \mathbf{L}_A^{(\varphi)}(t=l) | s') \\ \beta_{l+1}(s) &\triangleq \Pr(\mathbf{L}_A^{(\varphi)}(t > l) | s) \end{aligned}$$

We can write (3-7) as

$$\Pr(s_l = s', s_{l+1} = s, \mathbf{L}_A^{(\varphi)}) = \beta_{l+1}(s) \cdot \gamma_l(s', s) \cdot \alpha_l(s') \quad (3-8)$$

, and we can write the *branch metric*  $\gamma_l(s', s)$  as



$$\begin{aligned}
\gamma_l(\mathbf{s}', \mathbf{s}) &\triangleq \Pr(\mathbf{s}, \mathbf{L}_A^{(\varphi)}(t=l) | \mathbf{s}') \\
&= \left[ \frac{\Pr(\mathbf{s}', \mathbf{s})}{\Pr(\mathbf{s}')} \right] \left[ \frac{\Pr(\mathbf{s}', \mathbf{s}, \mathbf{L}_A^{(\varphi)}(t=l))}{\Pr(\mathbf{s}', \mathbf{s})} \right] \\
&= \Pr(\mathbf{s} | \mathbf{s}') \Pr(\mathbf{L}_A^{(\varphi)}(t=l) | \mathbf{s}', \mathbf{s}) \\
&= \Pr(\mathbf{s} | \mathbf{s}') \prod_{j=0}^{k-1} \Pr(L_A^{(\varphi)}(c_j) | c_j)
\end{aligned} \tag{3-9}$$

Where

$$\begin{aligned}
\Pr(L_A^{(\varphi)}(c_j) | c_j = 1) &= \frac{\exp(L_A^{(\varphi)}(c_j))}{1 + \exp(L_A^{(\varphi)}(c_j))} \\
\Pr(L_A^{(\varphi)}(c_j) | c_j = 0) &= \frac{1}{1 + \exp(L_A^{(\varphi)}(c_j))}
\end{aligned}$$

Thus, we can compute a *forward metric*  $\alpha_{l+1}(\mathbf{s}')$  for each state  $\mathbf{s}'$  at time  $l+1$  using the *forward recursion* method as

$$\begin{aligned}
\alpha_{l+1}(\mathbf{s}') &= \Pr(\mathbf{s}', \mathbf{L}_A^{(\varphi)}(t < l+1)) = \sum_{\mathbf{s} \in \sigma_l} \Pr(\mathbf{s}, \mathbf{s}', \mathbf{L}_A^{(\varphi)}(t < l+1)) \\
&= \sum_{\mathbf{s} \in \sigma_l} \Pr(\mathbf{s}', \mathbf{L}_A^{(\varphi)}(t=l) | \mathbf{s}, \mathbf{L}_A^{(\varphi)}(t < l)) \Pr(\mathbf{s}, \mathbf{L}_A^{(\varphi)}(t < l)) \\
&= \sum_{\mathbf{s} \in \sigma_l} \Pr(\mathbf{s}', \mathbf{L}_A^{(\varphi)}(t=l) | \mathbf{s}) \Pr(\mathbf{s}, \mathbf{L}_A^{(\varphi)}(t < l)) \\
&= \sum_{\mathbf{s} \in \sigma_l} \gamma_l(\mathbf{s}', \mathbf{s}) \alpha_l(\mathbf{s}')
\end{aligned} \tag{3-10}$$

Where  $\sigma_l$  is the set of all states at time  $l$ . A *backward metric*  $\beta_l(\mathbf{s})$  for each state  $\mathbf{s}$  at time  $l$  using the *backward recursion* method as

$$\begin{aligned}
\beta_{l+1}(\mathbf{s}) &\triangleq \Pr(\mathbf{L}_A^{(\varphi)}(t > l) | \mathbf{s}) = \sum_{\mathbf{s}' \in \sigma_{l+2}} \Pr(\mathbf{L}_A^{(\varphi)}(t > l), \mathbf{s}_{l+2} = \mathbf{s}' | \mathbf{s}_{l+1} = \mathbf{s}) \\
&= \sum_{\mathbf{s}' \in \sigma_{l+1}} \Pr(\mathbf{L}_A^{(\varphi)}(t=l+1), \mathbf{s}_{l+2} = \mathbf{s}' | \mathbf{s}_{l+1} = \mathbf{s}) \Pr(\mathbf{L}_A^{(\varphi)}(t > l+1) | \mathbf{s}_{l+1} = \mathbf{s}) \\
&= \sum_{\mathbf{s}' \in \sigma_{l+1}} \gamma_{l+1}(\mathbf{s}', \mathbf{s}) \beta_{l+2}(\mathbf{s}')
\end{aligned} \tag{3-11}$$

Therefore, according to equation (3-9), (3-10), and (3-11), the log-APP of coded bit  $c_j$  can be written as

$$\begin{aligned}
L_D^{(\varphi)}(c_j) &= \log \frac{\sum_{(s',s) \in \Sigma_l^1} \beta_{l+1}(s) \cdot \gamma_l(s',s) \cdot \alpha_l(s')}{\sum_{(s',s) \in \Sigma_l^0} \beta_{l+1}(s) \cdot \gamma_l(s',s) \cdot \alpha_l(s')} \\
&= \log \frac{\sum_{(s',s) \in \Sigma_l^1} \beta_{l+1}(s) \cdot \alpha_l(s') \cdot \Pr(s|s') \prod_{i=0}^{k-1} \Pr(L_A^{(\varphi)}(c_i)|c_i)}{\sum_{(s',s) \in \Sigma_l^0} \beta_{l+1}(s) \cdot \alpha_l(s') \cdot \Pr(s|s') \prod_{i=0}^{k-1} \Pr(L_A^{(\varphi)}(c_i)|c_i)} \\
&= \log \frac{\Pr(L_A^{(\varphi)}(c_j)|c_j=1)}{\Pr(L_A^{(\varphi)}(c_j)|c_j=0)} + \log \frac{\sum_{(s',s) \in \Sigma_l^1} \beta_{l+1}(s) \cdot \alpha_l(s') \cdot \Pr(s|s') \prod_{\substack{i=0 \\ i \neq j}}^{k-1} \Pr(L_A^{(\varphi)}(c_i)|c_i)}{\sum_{(s',s) \in \Sigma_l^0} \beta_{l+1}(s) \cdot \alpha_l(s') \cdot \Pr(s|s') \prod_{\substack{i=0 \\ i \neq j}}^{k-1} \Pr(L_A^{(\varphi)}(c_i)|c_i)} \\
&= L_A^{(\varphi)}(c_j) + L_E^{(\varphi)}(c_j) \tag{3-12}
\end{aligned}$$

The extrinsic LLRs are then passed to detector for next iteration of processing.

After iteratively processing is terminated, we decode information bits by using a posteriori LLRs with hard decision. The a posteriori LLRs of information bit  $b_n$  is

$$L_D(b_n) = \log \frac{\sum_{(s',s) \in \Omega_l^1} \beta_{l+1}(s) \cdot \gamma_l(s',s) \cdot \alpha_l(s')}{\sum_{(s',s) \in \Omega_l^0} \beta_{l+1}(s) \cdot \gamma_l(s',s) \cdot \alpha_l(s')} \tag{3-13}$$

where  $\Omega_l^b$  is the set of state pairs that corresponds to the information bit  $b_n = b$  at time  $l$ . And we decode information bits as

$$\hat{b}_n = \begin{cases} 1 & , L_D(b_n) > 0 \\ 0 & , L_D(b_n) \leq 0 \end{cases} \tag{3-14}$$

In order to simplify the calculations, the following identity is used

$$\max^*(x, y) \triangleq \log(e^x + e^y) = \max(x, y) + \log(1 + e^{-|x-y|}) \tag{3-15}$$

and we define the log-domain metrics as

$$\begin{aligned}\alpha_l^*(s') &= \log(\alpha_l(s')) \\ \gamma_l^*(s', s) &= \log(\gamma_l(s', s)) \\ \beta_{l+1}^*(s) &= \log(\beta_{l+1}(s))\end{aligned}$$

Finally by using the log-domain metrics, the e.q. (3-13) can be written as

$$\begin{aligned}L_D(b_n) &= \log \frac{\sum_{(s', s) \in \Omega_1^l} \beta_{l+1}(s) \cdot \gamma_l(s', s) \cdot \alpha_l(s')}{\sum_{(s', s) \in \Omega_0^l} \beta_{l+1}(s) \cdot \gamma_l(s', s) \cdot \alpha_l(s')} \\ &= \max_{(s', s) \in \Omega_1^l}^* \{ \beta_{l+1}^*(s) + \gamma_l^*(s', s) + \alpha_l^*(s') \} - \\ &\quad \max_{(s', s) \in \Omega_0^l}^* \{ \beta_{l+1}^*(s) + \gamma_l^*(s', s) + \alpha_l^*(s') \}\end{aligned} \quad (3.16)$$

The exponential terms in e.q. (3-13) have been convert to addition terms in e.q. (3-16) , and the complexity is reduced largely. To reduce computation complexity further, the “max\* “ function can be approximated as

$$\max^*(x, y) \approx \max(x, y) \quad (3-15)$$

the decoder using the function max instead of max\* is called *max-log-MAP* decoder. In the rests of this thesis, we consider only the *max-log-MAP* decoder for practical reason.

## Chapter 4 : Extrinsic Information Transfer Curve (EXIT)

### Chart

In this chapter, we discuss a powerful tool, the EXIT chart, and use it to analyze the convergence behavior of iterative decoding. EXIT chart was proposed by S. ten Brink in 2001. EXIT chart depicts the relation between mutual information of intrinsic log-likelihood ratios and coded bits and that of extrinsic log-likelihood ratios and coded bits for soft input soft output (SISO) decoder (or detector). Using mutual information transfer characteristics of SISO decoder, we can analyze the convergence behavior and design the system for better performance.

#### 4.1.1 : Transfer Characteristic

A SISO system is shown in Fig. 4.1. Where  $\mathbf{X}$  is the information we transmit, that is, coded bits sequence in BICM-ID system,  $L_A$  is intrinsic soft information and  $L_E$  is extrinsic soft information about  $\mathbf{X}$ .

First, we consider a simple case of BPSK modulation over AWGN channel. The received signal is

$$y = x + n \quad (4.1)$$

where “x” is the transmitted BPSK signal and “n” is AWGN noise with zero mean and variance  $\sigma_n^2$ . At receiver, the log-likelihood ratio is calculated as

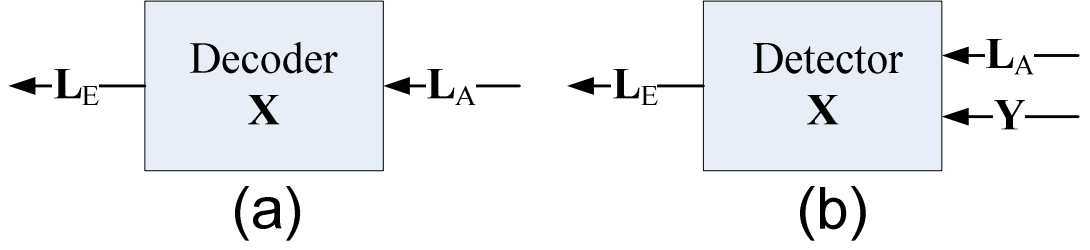


Fig. 4.1 Soft-input-soft-output (SISO) decoder (a) and detector (b)

$$L = \log \frac{\Pr(y|x=+1)}{\Pr(y|x=-1)} = \log \frac{\frac{1}{\sqrt{2\pi\sigma_n}} \exp\left(-\frac{(y-1)^2}{2\sigma_n^2}\right)}{\frac{1}{\sqrt{2\pi\sigma_n}} \exp\left(-\frac{(y+1)^2}{2\sigma_n^2}\right)} \quad (4.2)$$

$$= \frac{2}{\sigma_n^2} \cdot y = \frac{2}{\sigma_n^2} (x + n) = \mu_y \cdot x + n_y$$

where  $\mu_y = \frac{2}{\sigma_n^2}$  and  $n_y$  is Gaussian distribution with zero mean and variance

$$\sigma_y^2 = 2\mu_y.$$

Two observations in [9] are used :

- (1) For large inter-leavers the a priori values  $L_A$  remain fairly uncorrelated from the respective channel observation over much iteration.
- (2) The probability density functions of the extrinsic values  $L_E$  approach Gaussian-like distributions with increasing number of iterations.

Observations 1 and 2 suggest that the intrinsic soft information input to detector or decoder can be modeled by an independent Gaussian random variable as

$$L_A = \mu_A x + n_A, \quad n_A \sim N(0, \sigma_A^2) \quad , 2\mu_A = \sigma_A^2$$

therefore, the conditional PDF of  $L_A$  is :

$$p_A(\xi|X=x) = \frac{1}{\sqrt{2\pi}\sigma_A} \exp\left(-\frac{\left(\xi - \frac{\sigma_A^2}{2}x\right)^2}{2\sigma_A^2}\right) \quad (4.3)$$

The mutual information between transmission bit  $x$  and intrinsic LLR  $a$  is calculated as

$$I_A = I(X; A) = \frac{1}{2} \sum_{x=\pm 1} \int_{-\infty}^{+\infty} P_A(\xi|X=x) \log_2 \frac{2 \cdot P_A(\xi|X=x)}{P_A(\xi|X=+1) + P_A(\xi|X=-1)} d\xi \quad (4.4)$$

With equation (4.3), we rewrite  $I_A$  as a function of  $\sigma_A$

$$I_A(\sigma_A) = 1 - \int_{-\infty}^{+\infty} \frac{\exp\left(-\left(\xi - \frac{\sigma_A^2}{2}\right)^2 / 2\sigma_A^2\right)}{\sqrt{2\pi}\sigma_A} \log_2(1 + \exp(-\xi)) d\xi \quad (4.5)$$

Fig. 4.2 shows the relation between  $I_A$  and  $\sigma_A$

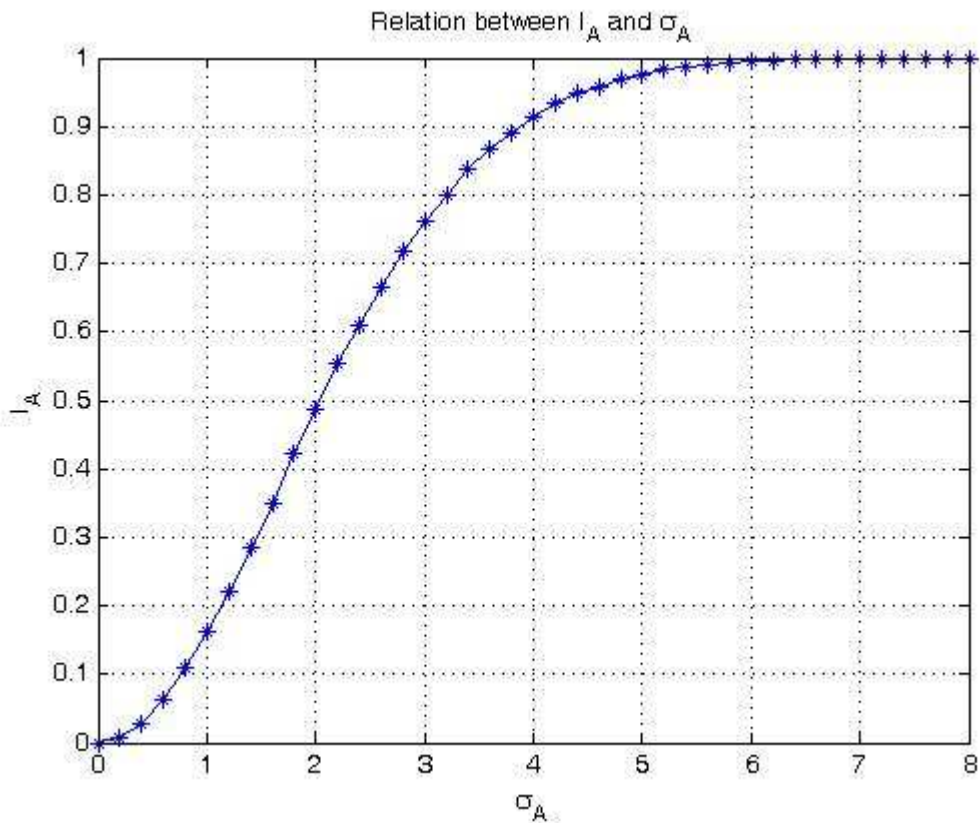


Fig. 4.2 the relation between  $I_A$  and  $\sigma_A$

The mutual information between extrinsic output  $E$  and transmission bit  $x$  can be

calculated as

$$I_E = I(X; E) = \frac{1}{2} \sum_{x=\pm 1} \int_{-\infty}^{+\infty} P_E(\xi|X=x) \log_2 \frac{2 \cdot P_A(\xi|X=x)}{P_E(\xi|X=+1) + P_E(\xi|X=-1)} d\xi \quad (4.6)$$

To compute  $I_E$  for a desired  $I_A$ , first we choose the  $\sigma_A$  according to  $I_A$  and model the intrinsic input as the independent Gaussian random variable in (4.6). Finally, we measure the mutual information between extrinsic outputs and transmission bits.

### 4.1.2 : Transfer Curve of Decoder

In BICM-ID system, the outer decoder receives the log-likelihood ratios from the detector. Hence, the transfer curve of decoder only influenced by the error correction code we use.

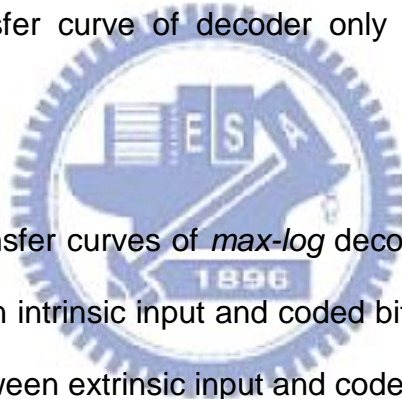


Fig. 4.3 shows several transfer curves of *max-log* decoders. In EXIT Chart, the mutual information between intrinsic input and coded bits is plot on “X” axis and the mutual information between extrinsic input and coded bits is plot on “Y” axis.

It is obvious for all the decoders that the a more reliable intrinsic inputs to decoder the more reliable extrinsic the decoder outputs. In Fig. 4.3, we can see that the threshold of the extrinsic is more apparent if the code with more powerful error correcting capability. Take turbo code with eight inner iterations for instance, If the mutual information of coded bits and intrinsic is over than 0.5, the mutual information of coded bits and extrinsic increases dramatically.

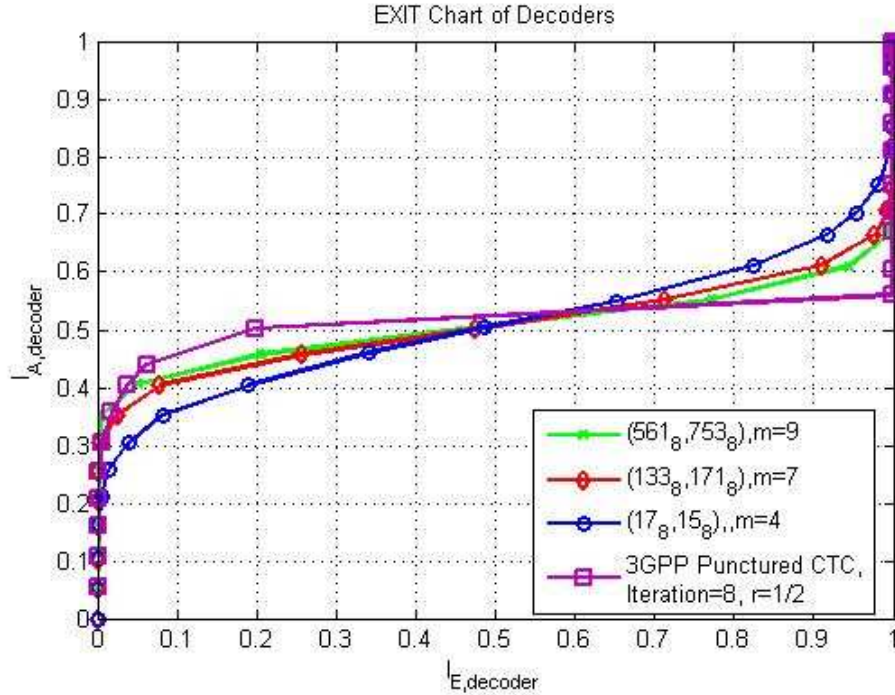


Fig. 4.3 Transfer curves of several convolutional code with distinct constrain length and of 3GPP turbo code

### 4.1.3 : Transfer Curve of Detector

As shown in Fig. 4.4, the detector receives both the log-likelihood ratios ( $l_a$ ) from the decoder and signals ( $y_1, \dots, y_T$ ) from communication channel. Random variables are written using upper case letters and their realizations by the corresponding lower case ones. Therefore, the mutual information can be written as

$$I_A = I(\mathbf{S}; \mathbf{L}_A) = \frac{1}{m} \sum_{k=0}^{m-1} I(X_k; L_{A,k}) = \frac{1}{2} \sum_{c=0}^1 \int_{-\infty}^{+\infty} p(l_a|c) \log \left( \frac{p(l_a|c)}{p(l_a)} \right) dl_a \quad (4.7)$$

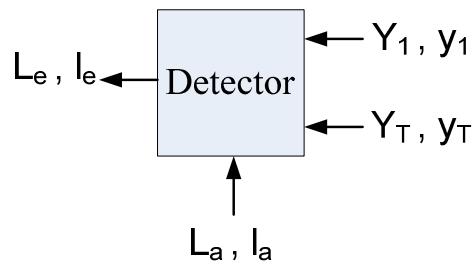


Fig. 4.4 Block diagram of detector ( demapper )



where  $X_k$  is  $k$ -th bit of transmission label  $\mathbf{s}$  and  $L_{A,k}$  is the intrinsic LLR of  $X_k$ .

The last step is true because that the intrinsic LLRs are assumed as i.i.d. Gaussian distribution as chapter 4.1.1. The mutual information between extrinsic LLR and transmission label is written as

$$I_E = I(\mathbf{S}; \mathbf{L}_E) = \frac{1}{m} \sum_{k=0}^{m-1} I(X_k; L_{E,k}) = \frac{1}{m} \sum_{k=0}^{m-1} I(X_k; \mathbf{L}_A^{[k]}, Y_1, \dots, Y_T) \quad (4.8)$$

where  $L_{E,k}$  is extrinsic LLR of  $k$ -th bit and  $\mathbf{L}_A^{[k]}$  is  $m-1$ -tuple vector composed of the LLRs of a label except which of  $k$ -th bit. The last equation is due to the detector calculate  $L_{E,k}$  based on only  $\mathbf{L}_A^{[k]}$  and  $Y_1, \dots, Y_T$ .

$$\begin{aligned} & I(X_k; \mathbf{L}_A^{[k]}, Y_1, \dots, Y_T) \\ &= H(X_k) - H(X_k | \mathbf{L}_A^{[k]}, Y_1, \dots, Y_T) \\ &= 1 - \int \int \dots \int p(\mathbf{L}_A^{[k]}, y_1, \dots, y_T) h\left(p(x_k = 0 | \mathbf{L}_A^{[k]}, y_1, \dots, y_T)\right) d\mathbf{L}_A^{[k]} dy_1 \dots dy_T \\ &= 1 - \int \int \dots \int p(\mathbf{L}_A^{[k]}) p(y_1) \dots p(y_T) h\left(p(x_k = 0 | \mathbf{L}_A^{[k]}, y_1, \dots, y_T)\right) d\mathbf{L}_A^{[k]} dy_1 \dots dy_T \end{aligned} \quad (4.9)$$

where  $h(p) = -p \log_2(p) - (1-p) \log_2(1-p)$  is the binary entropy function. The last step is true because the transmission bits are symmetric, that is,  $p(x_k = 0) = p(x_k = 1) = 0.5$ . With Bayes's theorem,  $p(x_k = 0 | \mathbf{L}_A^{[k]}, y_1, \dots, y_T)$  can be written as

$$\begin{aligned} & p(x_k = 0 | \mathbf{L}_A^{[k]}, y_1, \dots, y_T) \\ &= \frac{p(\mathbf{L}_A^{[k]}, y_1, \dots, y_T | x_k = 0) p(x_k = 0)}{\sum_{c=0}^1 p(\mathbf{L}_A^{[k]}, y_1, \dots, y_T | x_k = c) p(x_k = c)} \\ &= \frac{p(\mathbf{L}_A^{[k]}, y_1, \dots, y_T | x_k = 0)}{\sum_{c=0}^1 p(\mathbf{L}_A^{[k]}, y_1, \dots, y_T | x_k = c)} \end{aligned} \quad (4.10)$$

Therefore

$$\begin{aligned}
& p(\mathbf{I}_A^{[k]}, y_1, \dots, y_T | x_k = c) \\
&= \sum_{\mathbf{s} \in \Lambda} p(\mathbf{I}_A^{[k]}, y_1, \dots, y_T | \mathbf{s}, x_k = c) p(\mathbf{s} | x_k = c) \\
&= \sum_{\mathbf{s} \in \Lambda_k^c} p(\mathbf{I}_A^{[k]}, y_1, \dots, y_T | \mathbf{s}) p(\mathbf{s} | x_k = c) \quad (4.11) \\
&= \frac{2}{M} \sum_{\mathbf{s} \in \Lambda_k^c} p(y_1 | \mathbf{s}) \cdots p(y_T | \mathbf{s}) p(\mathbf{I}_A^{[k]} | \mathbf{s}) \\
&= \frac{2}{M} \sum_{\mathbf{s} \in \Lambda_k^c} p(y_1 | \mathbf{s}) \cdots p(y_T | \mathbf{s}) \prod_{\substack{i=0 \\ i \neq k}}^{m-1} p(l_{A,i} | c_j^s)
\end{aligned}$$

Using equations (4.7) ~ (4.11), the  $I_A$  and  $I_E$  can be calculated exactly but complicated since it needs to compute large integration. Because it is almost impossible to compute the exact value, Monte Carlo simulation (histogram measurements) is utilized.

From equation (4.11), we can observe that the channel condition and the mapping function are two key parameters that affect the EXIT chart of detector. Fig. 4.5 shows some results in [10] for AWGN and Rayleigh fading channels. With the observation that the transfer curves of chart of detector can be approximated to a straight lines, we define the “slope” of a transfer curve as the slope of the straight line from zero prior point ( $I_{A,\text{detector}} = 0$ ) to ideal prior point ( $I_{A,\text{detector}} = 1$ ). Mapping function set with various slope has been found in [10] for many regular modulation scheme.

Fig. 4.6 shows the transfer curves of Gray labeling under distinct channel condition (SNR). The transfer curves of identical labeling are approximately parallel, and the transfer curve is “higher” when SNR is larger.

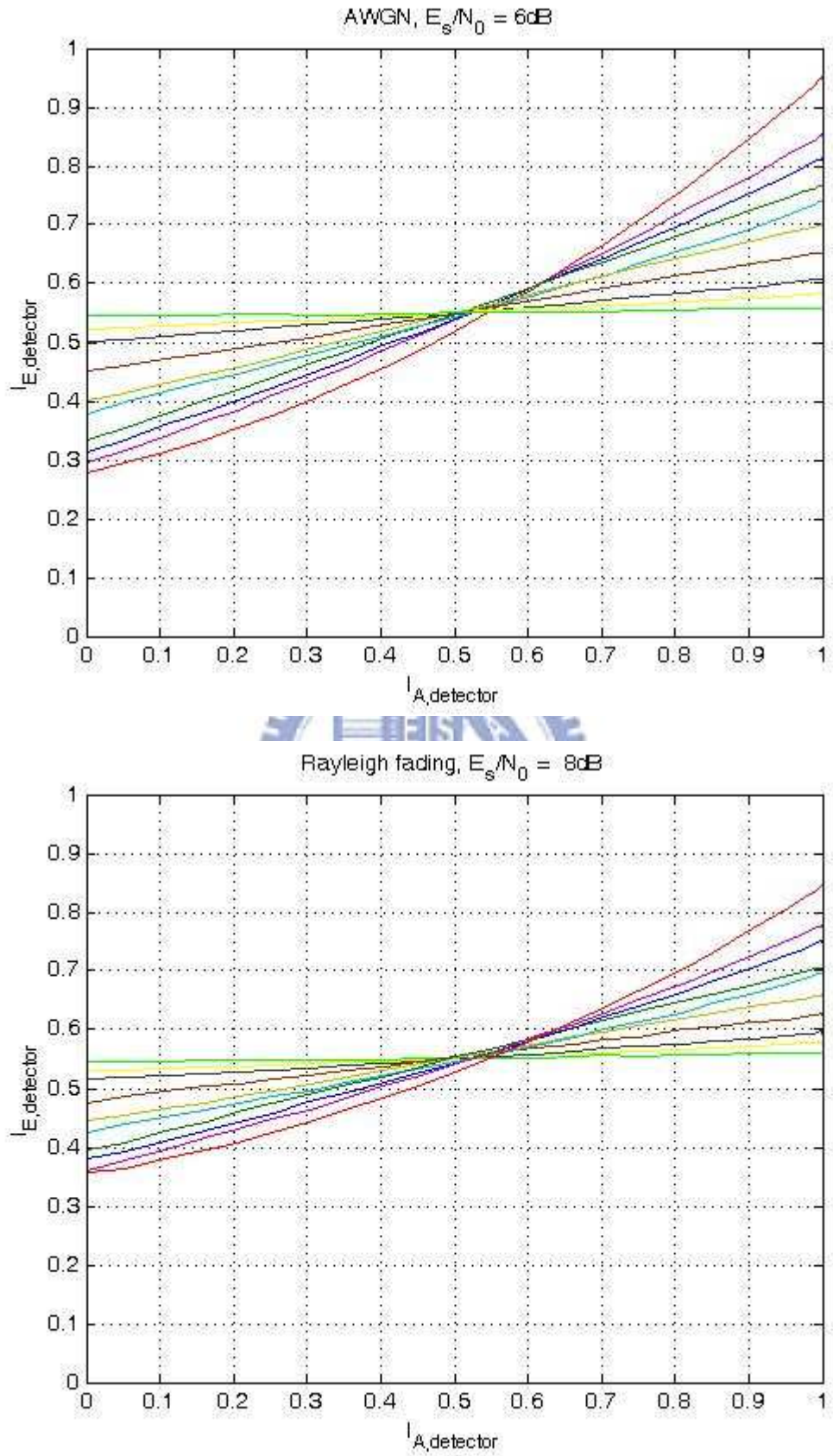


Fig. 4.5 Transfer curves of several labeling in AWGN and Rayleigh fading channel.

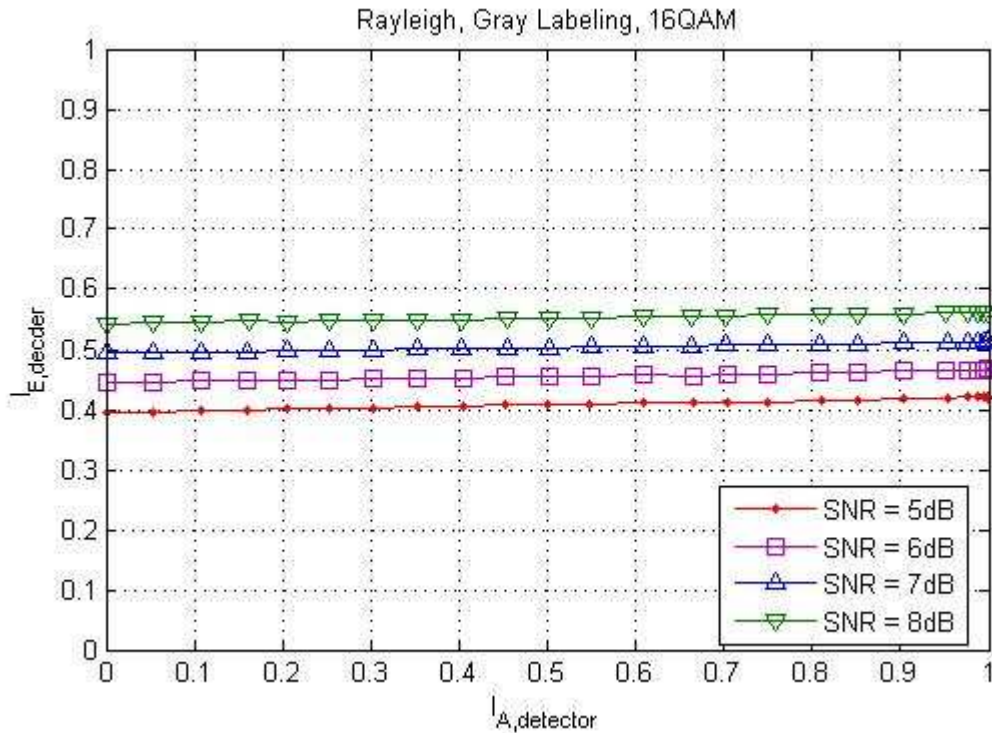


Fig. 4.6 Transfer curves of Gray labeling under distinct channel condition (SNR)

#### 4.1.4 : EXIT Chart

The EXIT chart is composed of transfer curves of detector and decoder. By EXIT chart, the behavior of extrinsic information during iterative decoding can be traced. Fig. 4.6 shows an example of EXIT Chart.

In Fig. 4.7, the decoder curve and the detector curve separate far enough to introduce a tunnel, the final extrinsic information of the decoder can reach the location with high reliability. In other word, the waterfall region on BER curve of iterative decoding is related to the appearance of the tunnel between detector transfer curve and decoder transfer curve. It is believed that the higher reliability of decoder output the lower bit error rate. In Fig 4.8, transfer curves of two distinct labeling under AWGN channel with identical SNR and the convolutional code are plotted. The “Blue” one intersects with the decoder transfer curve in the

point with low decoder extrinsic reliability, and the “Red” one introduce a tunnel between the detector and decoder. It is obvious that the red one has a better performance than the blue one.

Therefore, the criterion of choosing the suitable labeling is that the labeling with the tunnel appearing at as lower SNR as possible.



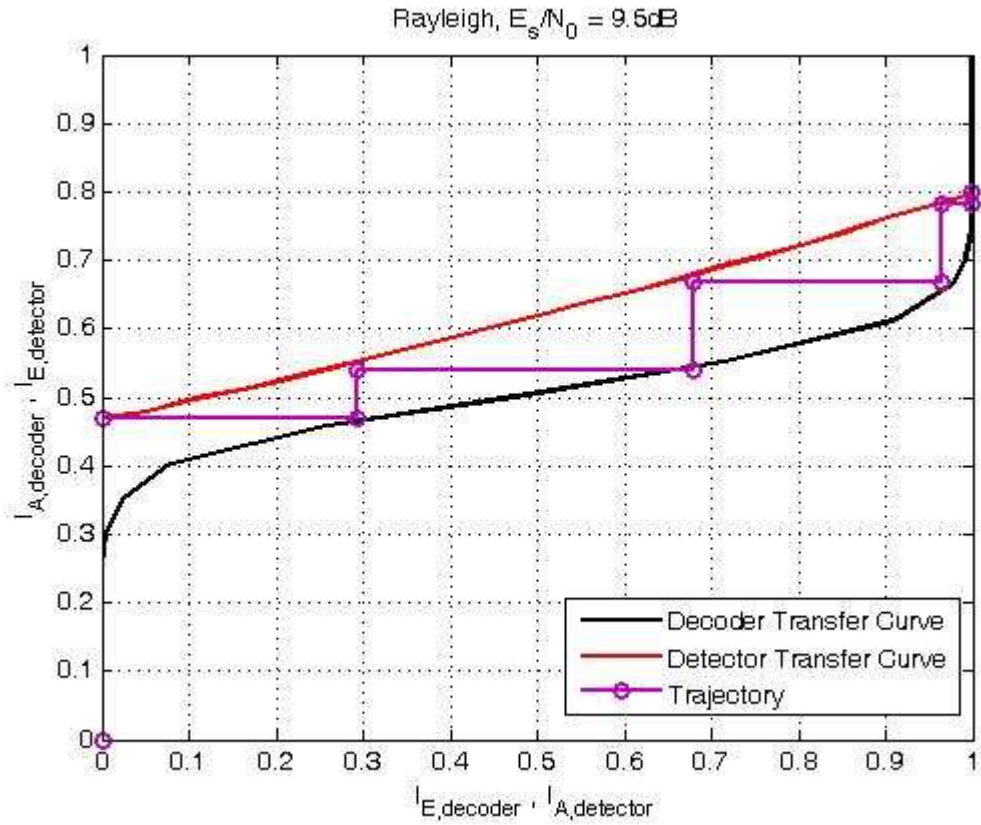


Fig. 4.7 Example of trajectory under iterative decoding

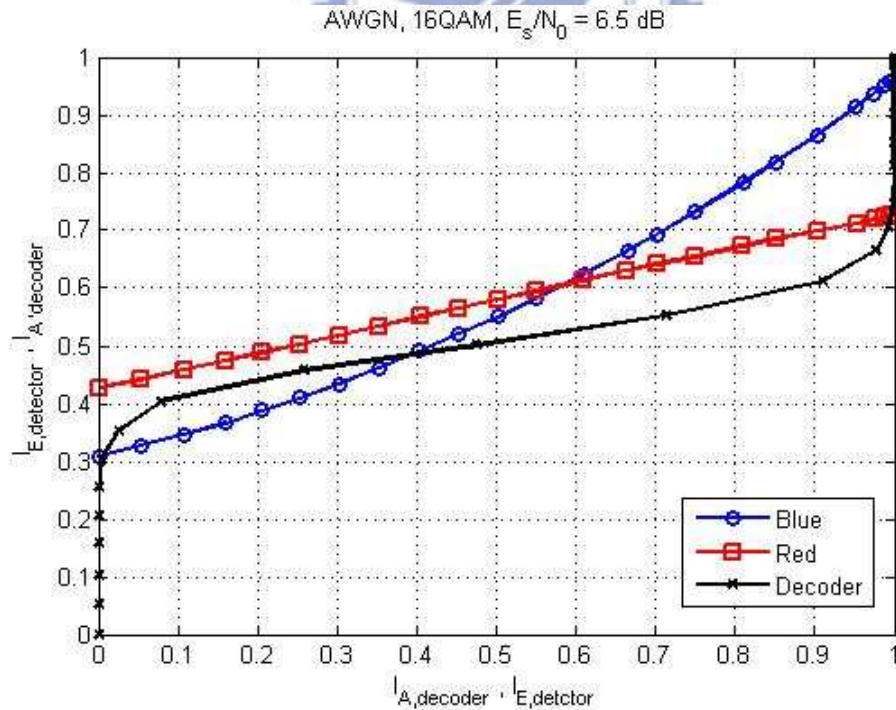


Fig. 4.8 Transfer curves of distinct labeling under identical channel condition (SNR)

## Chapter 5 : The Proposed Searching Algorithm

In the chapter, we propose an algorithm to search for labeling for Type-I HARQ in order to make throughput as high as possible. First, an analytical model for EXIT Chart is introduced. With the simple model, the detector transfer curve on EXIT could be approximated accurately by a close-form function. Next, we propose a search algorithm using the concept of binary search algorithm (BSA) to establish a labeling set. Therefore, optimal labeling can be chosen according to code scheme and SNR.

### 5.1 Simplified Model

An analytical approximate expression for the EXIT function of a maximum a posterior probability (MAP) detector over memory-less channels under single transmission is derived in [15]. The real communication channel is replaced with a hard decision virtual channel, and the intrinsic information coming from decoder is modeled as a binary symmetric channel or a binary erasure channel. The method is modified to the case of HARQ (Multiple transmissions) .

#### 5.1.1 Hard Decision Virtual Channel

The real communication channels considered in the thesis are AWGN and Rayleigh fading channels. Relation between transmit and receive signals can be represented as

$$y = h \cdot \sqrt{\gamma} \cdot x + n \quad (5.1)$$

where  $x$  is the transmitted constellation point and  $y$  is the corresponding received signal.  $h$  is the fading coefficient with distribution  $f_H(h) = 2h \exp(-h^2)$

in Rayleigh fading channel and  $h=1$  in AWGN channel.  $\gamma$  is the signal to noise ratio  $\frac{E_s}{N_0}$ , and  $n$  is *i.i.d.* complex Gaussian noise with distribution  $CN(0,1)$ .

Next, define a transmission matrix  $\mathbf{Q}^{M \times M}(\gamma)$  to characterize this virtual channel when SNR equal to  $\gamma$ . The element  $q_{i,j}$  denote transmission probability from the input signal  $x_i$  to received signal  $x_j$  if we use maximum likelihood (ML) detection on the received signal and hard decision,  $q_{i,j} = p(x^r = x_j | x^t = x_i)$   $x_j, x_i \in \mathcal{X}$ ,  $i, j = 0, 1, \dots, M-1$ . Obviously, the alphabet of output signals from real communication channel is infinite but which from virtual channel is finite. The capacity of this virtual channel is

$$\begin{aligned}
C_{hard}(\gamma) &= I(X^t; X^r) = \sum_{i=0}^{M-1} \sum_{j=0}^{M-1} p(X^t = x_i, X^r = x_j) \log_2 \left( \frac{p(X^t = x_i, X^r = x_j)}{p(X^t = x_i) p(X^r = x_j)} \right) \\
&= \sum_{i=0}^{M-1} \sum_{j=0}^{M-1} p(X^t = x_i, X^r = x_j) \log_2 \left( \frac{p(X^t = x_i, X^r = x_j)}{\sum_{k=0}^{M-1} p(X^r = x_j | X^t = x_k) p(X^t = x_k)} \right) \\
&= \sum_{i=0}^{M-1} \sum_{j=0}^{M-1} p(X^t = x_i, X^r = x_j) \log_2 (1/p(X^t = x_i)) + \\
&\quad \sum_{i=0}^{M-1} \sum_{j=0}^{M-1} p(X^t = x_i, X^r = x_j) p(X^t = x_i) \log_2 \left( \frac{p(X^t = x_i, X^r = x_j)}{\sum_{k=0}^{M-1} p(X^r = x_j | X^t = x_k)} \right) \\
&= \log_2(M) + \frac{1}{M} \sum_{i=0}^{M-1} \sum_{j=0}^{M-1} q_{i,j} \log_2 \left( \frac{q_{i,j}}{\sum_{k=0}^{M-1} q_{k,j}} \right) \tag{5.2}
\end{aligned}$$



where a constellation point is equally likely, that is,  $p(X^t = x_i) = \frac{1}{M}$ .

The capacity of real communication channel is

$$\begin{aligned}
C_{real}(\gamma) &= I(X^t; Y, H) \\
&= \sum_{i=0}^{M-1} \int \int p(X^t = x_i, y, h) \log_2 \left( \frac{p(X^t = x_i, y, h)}{p(X^t = x_i) p(y, h)} \right) dy dh \\
&= \sum_{i=0}^{M-1} \int \int p(x_i, y, h) \log_2 \left( \frac{1}{p(x_i)} \cdot \frac{p(x_i, y, h)}{p(y, h)} \right) dy dh \\
&= \log_2(M) + \sum_{i=0}^{M-1} \int \int p(y|x_i, h) p(x_i, h) \log_2 \left( \frac{p(y|x_i, h) p(x_i, h)}{\sum_{k=0}^{M-1} p(y|x_k, h) p(x_k, h)} \right) dy dh \\
&= \log_2(M) + \sum_{i=0}^{M-1} \int \int p(y|x_i, h) p(x_i, h) \log_2 \left( \frac{p(y|x_i, h)}{\sum_{k=0}^{M-1} p(y|x_k, h)} \right) dy dh \quad (5.3)
\end{aligned}$$

The last step in equation (5.3) follows that the probability of fading gain and transmitted signal are independent and transmitted signals are equally likely, that is,  $p(x_i, h) = p(x_i) p(h) = p(x_k) p(h) = p(x_k, h)$ ,  $\forall i, j = 0, \dots, M-1$ .

A number of capacities for 16-QAM constellations over AWGN and Rayleigh fading channels are plotted in Fig. 5.1 and Fig. 5.2. It is obviously that  $C_{hard}(\gamma) < C_{real}(\gamma)$ . In the simplified model, a discrete channel with transmission matrix  $\mathbf{Q}(\hat{\gamma})$  is selected instead of real communication channel with SNR equal to  $\gamma$  such that  $C_{hard}(\hat{\gamma}) = C_{real}(\gamma)$ .

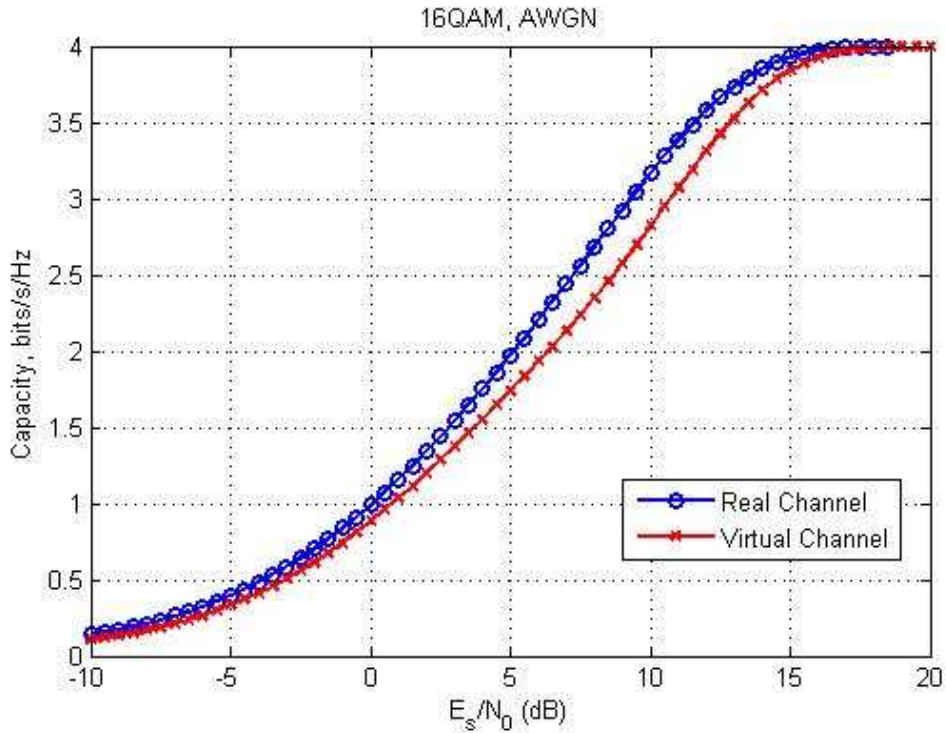


Fig. 5.1 Capacity for real communication channel and virtual channel (AWGN)

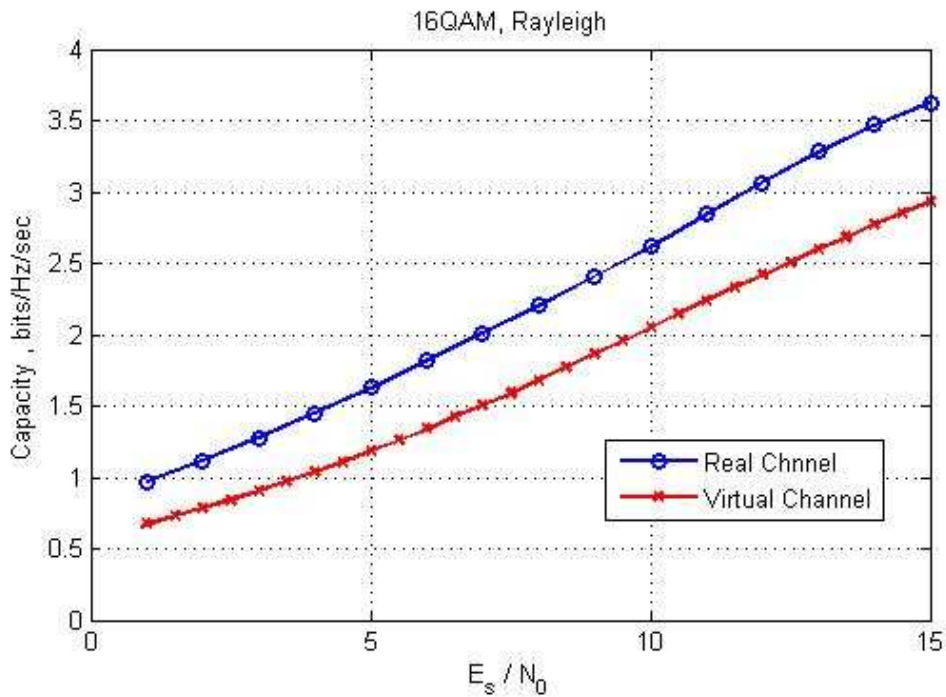


Fig. 5.2 Capacity for real communication channel and virtual channel (Rayleigh)

### 5.1.2 Binary Symmetric Extrinsic Channel

A BSC model is depicted in Fig. 5.3.  $b$  is the transmitted bit and  $l$  is the

corresponding extrinsic value from decoder which is served as prior in detector. The extrinsic value of any transmitted bit is either "0" or "1". The model is parameterized by the crossover probability  $\varepsilon$ . The transmitted bit is equally likely  $p(b=0) = p(b=1) = \frac{1}{2}$ , and it is obviously that  $p(l=0) = p(l=1) = \frac{1}{2}$ .

The mutual information between  $b$  and  $l$  can be calculated as

$$\begin{aligned}
 I(B;L) &= \sum_{b=0}^1 \sum_{l=0}^1 p(b,l) \log_2 \left( \frac{p(b,l)}{p(b)p(l)} \right) \\
 &= 1 + \sum_{b=0}^1 \sum_{l=0}^1 p(b,l) \log_2 (p(l|b)) \\
 &= 1 + (1-\varepsilon) \log(1-\varepsilon) + \varepsilon \log(\varepsilon) \tag{5.4} \\
 &= 1 - h(\varepsilon) \\
 h(\varepsilon) &= -(1-\varepsilon) \log(1-\varepsilon) - \varepsilon \log(\varepsilon)
 \end{aligned}$$

In the simplified model, the BSC extrinsic model is used instead of *i.i.d.* Gaussian model. A suitable  $\varepsilon$  is selected to introduce specific  $I_A$  in BSC model just like that we select  $\sigma_A$  in *i.i.d.* Gaussian model.

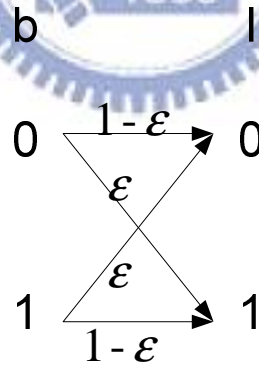


Fig. 5.3 Binary Symmetric Extrinsic Model

### 5.1.3 Closed-form EXIT function

The mutual information between coded bits and detector extrinsic has been derived in Section 4.1.3 for the communication channel with *i.i.d.* Gaussian prior. In the simplified model, the communication channel is replaced by a

discrete channel with transmission matrix  $Q$  and the *i.i.d.* Gaussian prior is replaced by a BSC extrinsic channel.

In the simplified model, therefore,  $I_A$  can be written as

$$I_A = 1 - h(\varepsilon) \quad (5.5)$$

and  $I_E$  can be written as

$$\begin{aligned} I_E &= I(\mathbf{S} ; \mathbf{L}_E) = \frac{1}{m} \sum_{k=0}^{m-1} I(X_k ; L_{E,k}) = \frac{1}{m} \sum_{k=0}^{m-1} I(X_k ; \mathbf{L}_A^{[k]}, Y_1, \dots, Y_T) \\ &= \frac{1}{m} \sum_{k=0}^{m-1} H(X_k) - H(X_k | \mathbf{L}_A^{[k]}, Y_1, \dots, Y_T) \\ &= \frac{1}{m} \sum_{k=0}^{m-1} \left\{ 1 - \sum_{\mathbf{l}_A^{[k]} \in \mathbf{P}} \sum_{y_1 \in \mathcal{Y}} \dots \sum_{y_T \in \mathcal{Y}} p(\mathbf{l}_A^{[k]}, y_1, \dots, y_T) h\left(p(x_k = 0 | \mathbf{l}_A^{[k]}, y_1, \dots, y_T)\right) \right\} \\ h(x) &= -(1-x) \log(1-x) - x \log x \end{aligned} \quad (5.6)$$

where  $\mathbf{P}$  is the set of all possible prior event and  $|\mathbf{P}| = 2^{m-1}$  in BSC model. Take eq. (4.10) and eq. (4.11) into eq. (5.6),  $I_E$  can be obtained easily and quickly.

Fig. 5.4 and Fig 5.5 show results for two and three multiple transmissions for 16QAM under Rayleigh fading channel. The results of simplified model are plotted with dotted lines, and those of real communication model are plotted with solid lines. We can see that there are only slightly different between two models. The simplified model for 8PSK is also derived and is vary accurate as is shown.

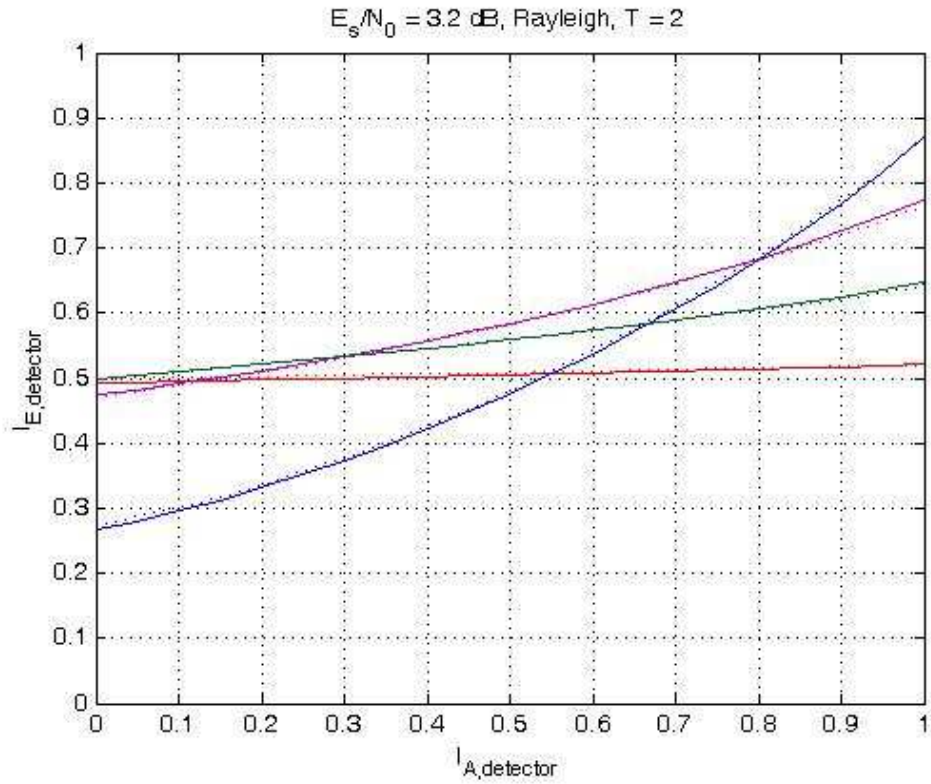


Fig. 5.4 Two transmissions for 16QAM under Rayleigh fading channel

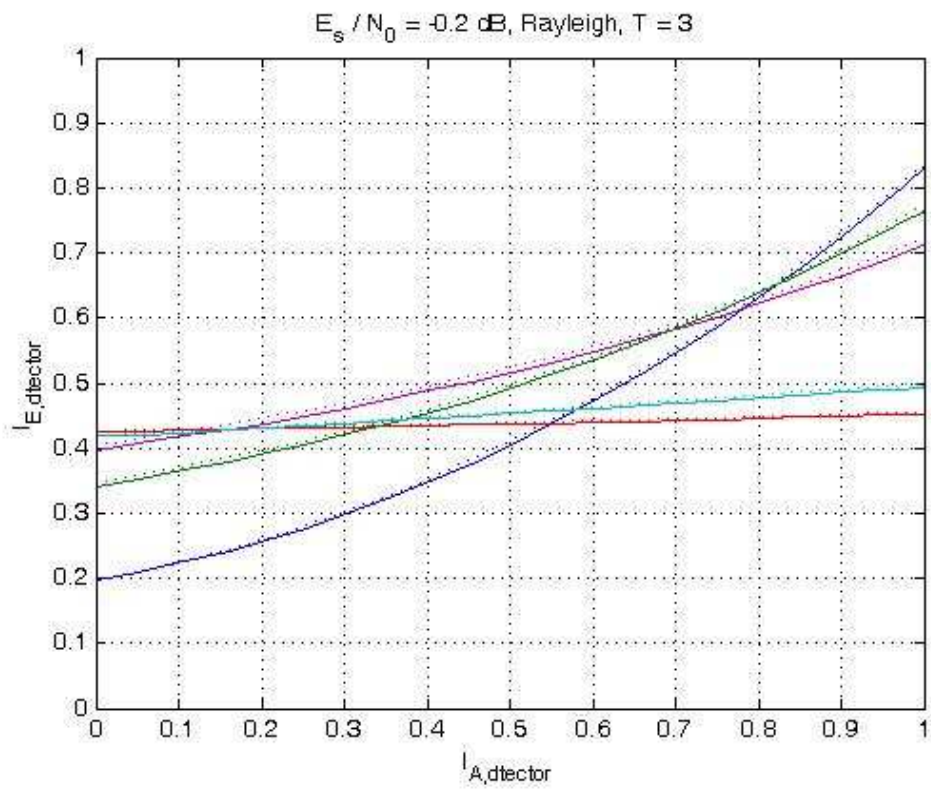


Fig. 5.5 Three transmissions for 16QAM under Rayleigh fading channel

## 5.2 Searching Algorithm

Consider a HARQ system, the mapping function for the first transmission can be one of the mapping function obtain in previous work [10] which is designed to match the outer code. Suppose the mapping functions of  $T-1$  transmissions have been known, we want to design the mapping function for  $T$  transmission,  $\mu^T(s)$ , based on mapping functions  $\mu^1(s), \dots, \mu^{T-1}(s)$ .

Define  $I_0^\gamma(\mu_1, \dots, \mu_T)$  is the mutual information between detector extrinsic and codeword under simplified model when the mutual information between detector intrinsic and codeword is equal to zero, that is, it relates to the leftist point on EXIT chart, and  $I_1^\gamma(\mu_1, \dots, \mu_T)$  is the mutual information between detector extrinsic and codeword under simplified model when the mutual information between detector intrinsic and codeword is equal to one, that is, it relates to the rightist point on EXIT chart. From observation, the detector transfer curve approaches a straight line. Therefore, a straight line from  $(0, I_0^\gamma(\mu_1, \dots, \mu_T))$  to  $(1, I_1^\gamma(\mu_1, \dots, \mu_T))$  is defined as a virtual transfer curve and the slope of the virtual transfer curve is defined as “*slope*” of the jointly-detected transfer curve of the mapping function pair  $\mu_1, \dots, \mu_T$ . Another reason to introduce the virtual transfer curve is that  $(0, I_0^\gamma(\mu_1, \dots, \mu_T))$  is the point that decides whether a tunnel exists between detector transfer curve and decoder curve such as the trajectory can stretch far away, and  $(1, I_1^\gamma(\mu_1, \dots, \mu_T))$  is the point decides the position of error flow. Hence, the two points on EXIT chart is what we are mostly

concerned.

Fig. 5.6 shows some results for the case that the maximum transmission number is equal to two. The first mapping function is fixed and the second one is selected base on the results in Fig. 5.6. It can be observed that the jointly-detected transfer curves of these mapping function pairs have similar *slopes* but different area under the curve. The best labeling set between those is the one with largest area under the curve because it makes the tunnel between the decoder transfer curve and detector transfer curve the widest. It concludes that the *slope* and *height* of transfer curve of detector are the most important characteristic that concerns us.

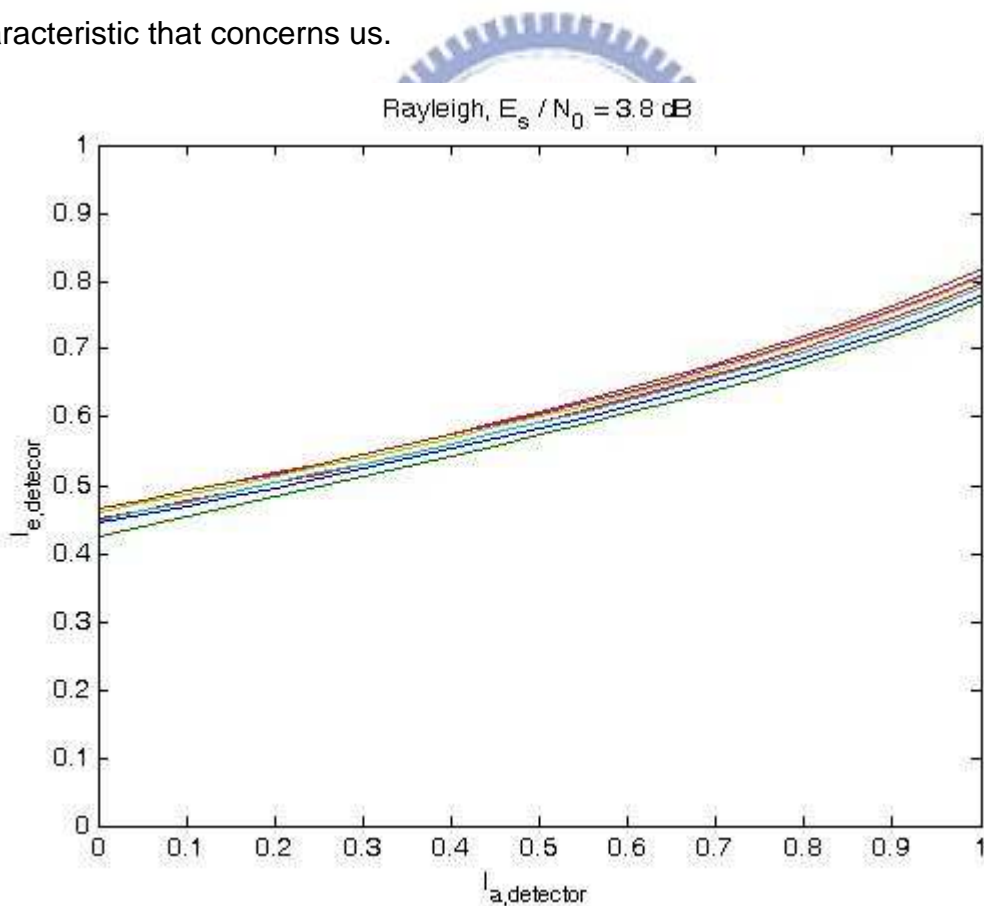


Fig. 5.6 Transfer curves of several labeling pair with fixed 1st mapping function

First, base on predetermined mapping functions  $\mu^1(s), \dots, \mu^{T-1}(s)$ , we set up a

table as table 5.1. Because the slope of detector curve is from 0 to 1, we quantize those uniformly to finite set  $\mathbf{M}$ ,  $|\mathbf{M}| = K$ , that is, in row  $k$ ,  $m_k$  is equal to  $\frac{k}{K}$ .  $\mu_k$  in row  $k$  is the mapping function such as

$$m_k = \arg \min_{m \in \mathbf{M}} \left\{ \left[ I_0^\gamma(\mu^1, \dots, \mu^{T-1}, \mu_k) - I_0^\gamma(\mu^1, \dots, \mu^{T-1}, m) \right] - m \right\}$$

$$D_{\mu_k} = I_0^\gamma(\mu^1, \dots, \mu^{T-1}, \mu_k) + I_0^\gamma(\mu^1, \dots, \mu^{T-1}, \mu_k)$$

namely,  $m_k$  is the quantized slope of virtual transfer curve of  $(\mu^1, \dots, \mu^{T-1}, \mu_k)$ , and  $D_{\mu_k}$  stand for the area under the virtual transfer curve because the altitude of the ladder-shaped area is equal to one.

	<b>M</b>	<b>D</b>	
⋮	⋮	⋮	⋮
$k$	$m_k$	$D_{\mu_k}$	$\mu_k$
⋮	⋮	⋮	⋮

Table 5.1 Table used for searching algorithm

**【Initial Step】**

Predetermine a number of initial seeds. A table is set up for each seed with every  $D_{\mu_k}$  value set to zero initially. An initial seed mapping function is given in this step sequentially.

**【Step. 1.】**

Compute all possible swaps of two indices for all seeds, and update the table belong to the initial seed. For instance, to deal with 3 seeds with 16QAM modulation, there are  $3 \cdot (16 \cdot 15 / 2) = 260$  possible swaps. The method to update the table listed as follow :

Suppose  $\Sigma$  is the set composed of all swaps, than compute all  $\mu \in \Sigma$



$$D = I_1(\mu^1, \dots, \mu^{T-1}, \mu) + I_0(\mu^1, \dots, \mu^{T-1}, \mu)$$

$$m' = I_1(\mu^1, \dots, \mu^{T-1}, \mu) - I_0(\mu^1, \dots, \mu^{T-1}, \mu)$$

$$m_k = \arg \min_{m \in M} (\|m' - m\|)$$

If ( $D > D_{\mu_k}$ )

*Update the table  $D_{\mu_k} = D$  and  $\mu_k = \mu$*

After all swaps have been calculated, go to *step. 2.*

**【Step. 2.】**

If (the table has been updated)

*Set the labels correspond to the updated rows as new seeds and return to Step. 1.*

if (the table has not been updated)

{

*The table related to this initial is kept.*

if (new initial seed is available)

*Pick a new initial seed with corresponding table and return to Step. 1.*

else

*Go to Step. 3*

}

**【Step. 3.】**

Compare all the tables related to each initial seed we obtained above.

We pick up the mapping functions with maximum  $D_{\mu_k}$  value among

each specific row  $k$  of all the tables. Those picked-up mapping

functions are formed a mapping function set of which detector transfer

with various slopes and largest area.

Perform searching algorithm depicted above, a mapping functions set for retransmission can be obtained sequentially. With the mapping functions set, link adaptation can be realized by that using distinct mapping function according to channel signal to noise ratio (SNR) .

### 5.3 Simulation Results

In this section, a set of mapping functions for retransmissions are obtained through the proposed searching algorithm. The performance of our design is compared with that of chase combining and previous labeling that is obtained with no consideration of the outer code. The parameters of simulation are listed below

<i>Coding scheme</i>	$(133_8, 171_8)$
<i>code rate</i>	$1/2$
<i>Modulation scheme</i>	16QAM, 8PSK
<i># of information bits</i>	2500
<i>BICM - ID Iteration (Outer Iteration)</i>	10

Table 5.2. Simulation parameter of CC  $(133_8, 171_8)$

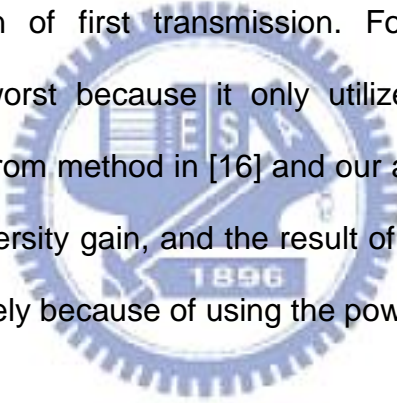
#### 5.3.1 CC $(133_8, 171_8)$ , 16QAM, Rayleigh channel

The optimal mapping function of first transmission for  $(133_8, 171_8)$  convolution code is picked from the labeling set in [10].

Base on the mapping function we search the mapping function for the second transmission using the proposed searching algorithm. The results are shown in Fig. 5.7 where two mapping functions are selected. It is observed that the two mapping function have different properties, for example the left point of the “red”

one is higher than the “pink” one, and we suppose the performance of “red” one is with better than that of the “pink” one at low SNR region. On the other hand, the “pink” one is better than the “red” one at high SNR region. The transfer functions for third transmission are based on the first mapping function and the second mapping function with “red” transfer curve.

Fig. 5.8 shows the throughput of our design, chase combining and the labeling obtained in [16]. In [16], the authors searched retransmission mapping function based on the BER upper bound under zero-prior and ideal-prior conditions and without considering outer code. We compare three HARQ strategies using identical mapping function of first transmission. For Fig. 5.8, the chase combining performs the worst because it only utilizes power gain with no diversity gain. The results from method in [16] and our algorithm both utilize the power gain and symbol diversity gain, and the result of our algorithm utilize the diversity gain more accurately because of using the powerful tool EXIT chart.



The best mapping function for a HARQ system with maximum transmission number 3 is sorted as

\s	0	1	2	3	4	5	6	7	8	9	10	11	12	13	14	15
$\mu_1(\mathbf{s})$	0	8	13	2	4	5	15	6	12	3	7	14	11	9	1	10
$\mu_{2,1}(\mathbf{s})$	7	14	8	15	9	3	11	12	6	2	10	13	5	1	4	0
$\mu_{2,2}(\mathbf{s})$	5	13	1	9	0	8	4	12	6	10	2	14	7	11	3	15
$\mu_{3,1}(\mathbf{s})$	7	8	13	3	4	14	11	0	2	9	6	5	15	1	12	10
$\mu_{3,2}(\mathbf{s})$	13	9	10	11	1	4	6	7	12	8	15	14	0	5	2	3

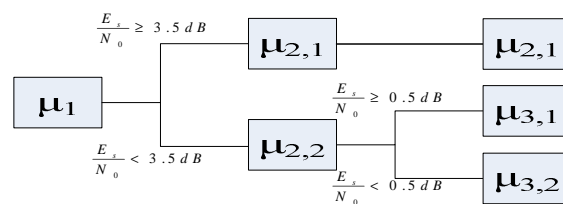


Table 5.3 Strategy of link adaptation for CC (133<sub>8</sub>, 171<sub>8</sub>) with 16-QAM

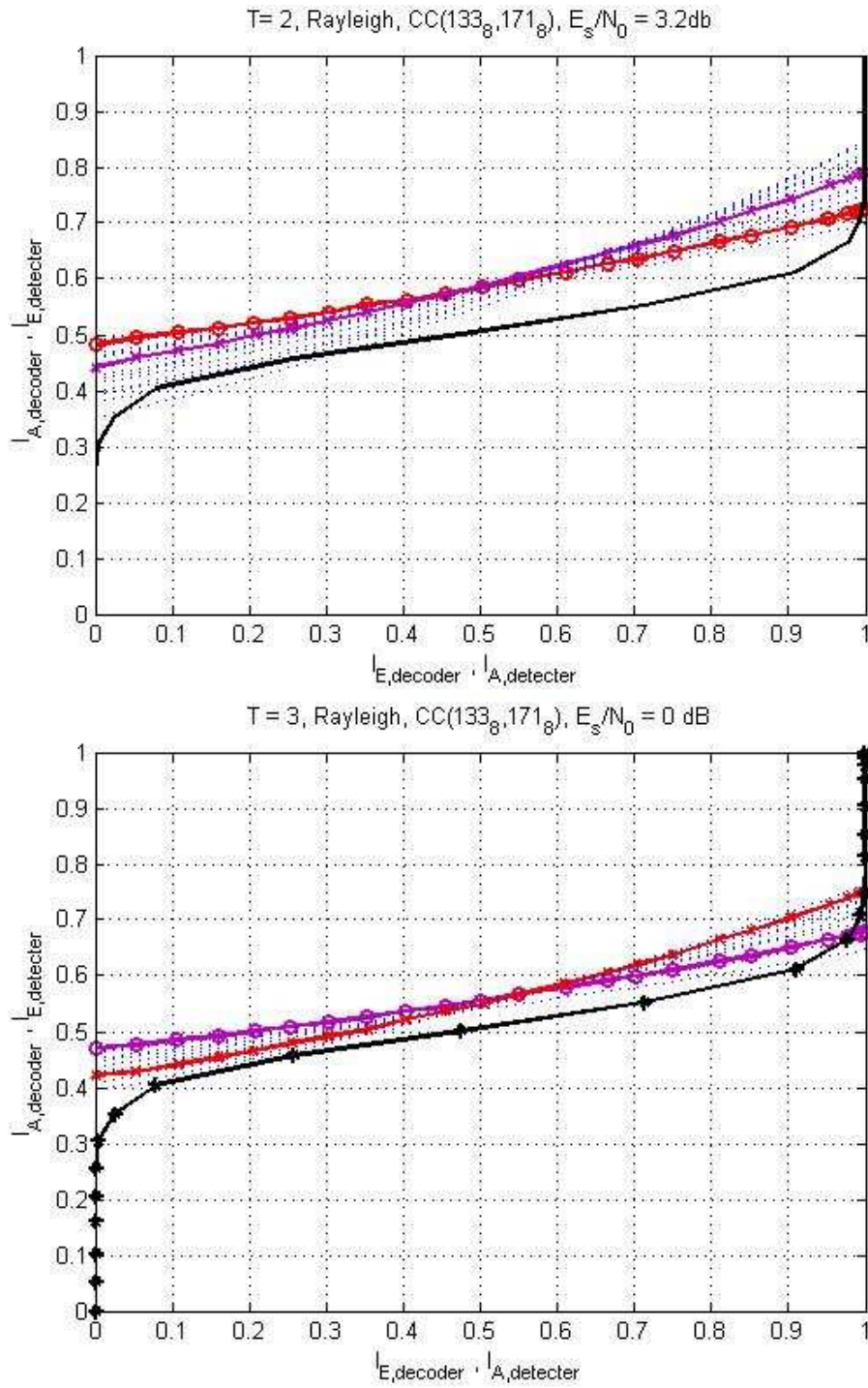


Fig. 5.7 Transfer curves of the suitable labeling in our design for CC( 133<sub>8</sub> , 171<sub>8</sub> ) with 16-QAM.

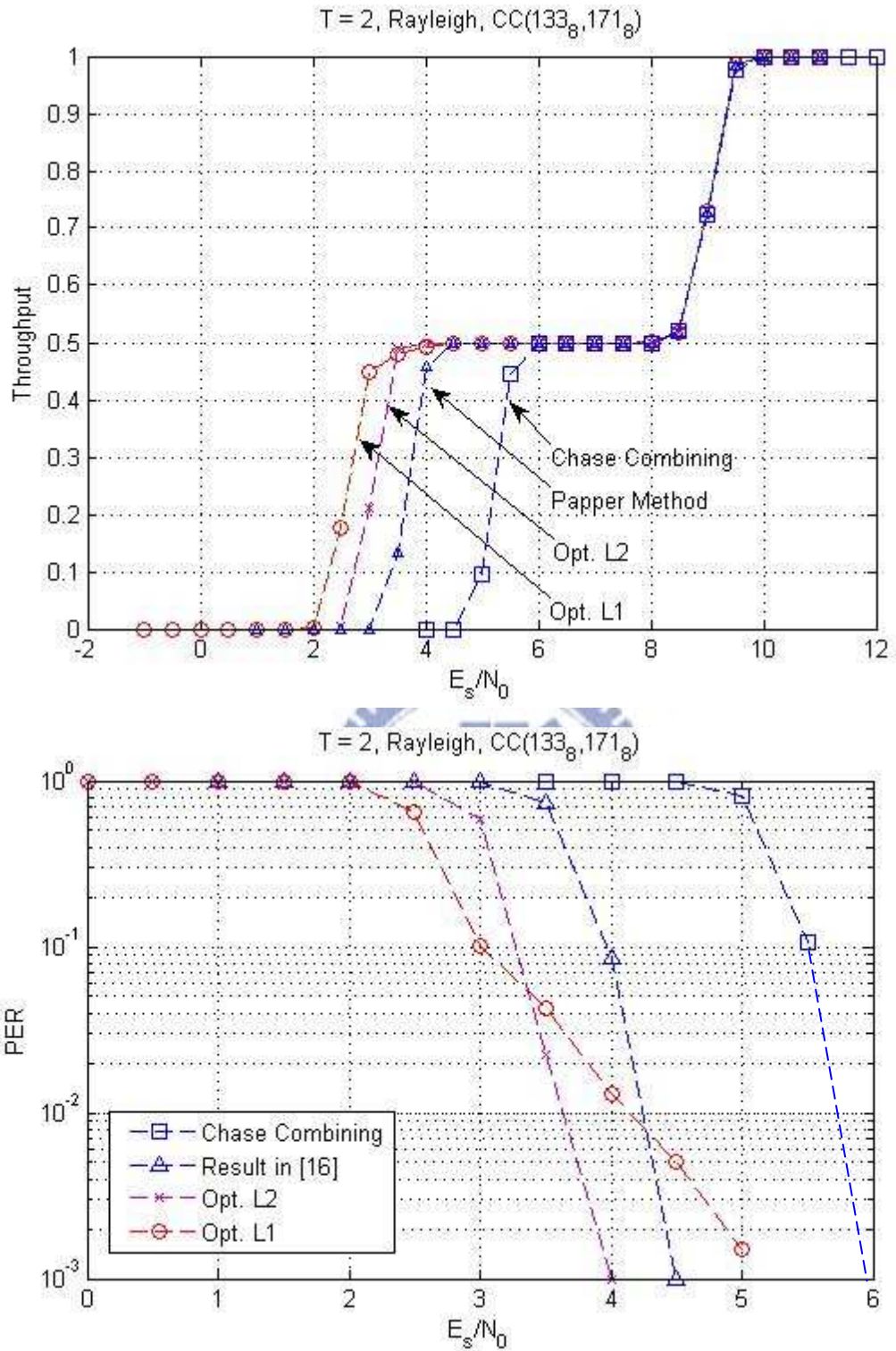


Fig. 5.8 Throughput and PER of the suitable labeling for CC (133<sub>8</sub>, 171<sub>8</sub>) with 16-QAM under T = 2

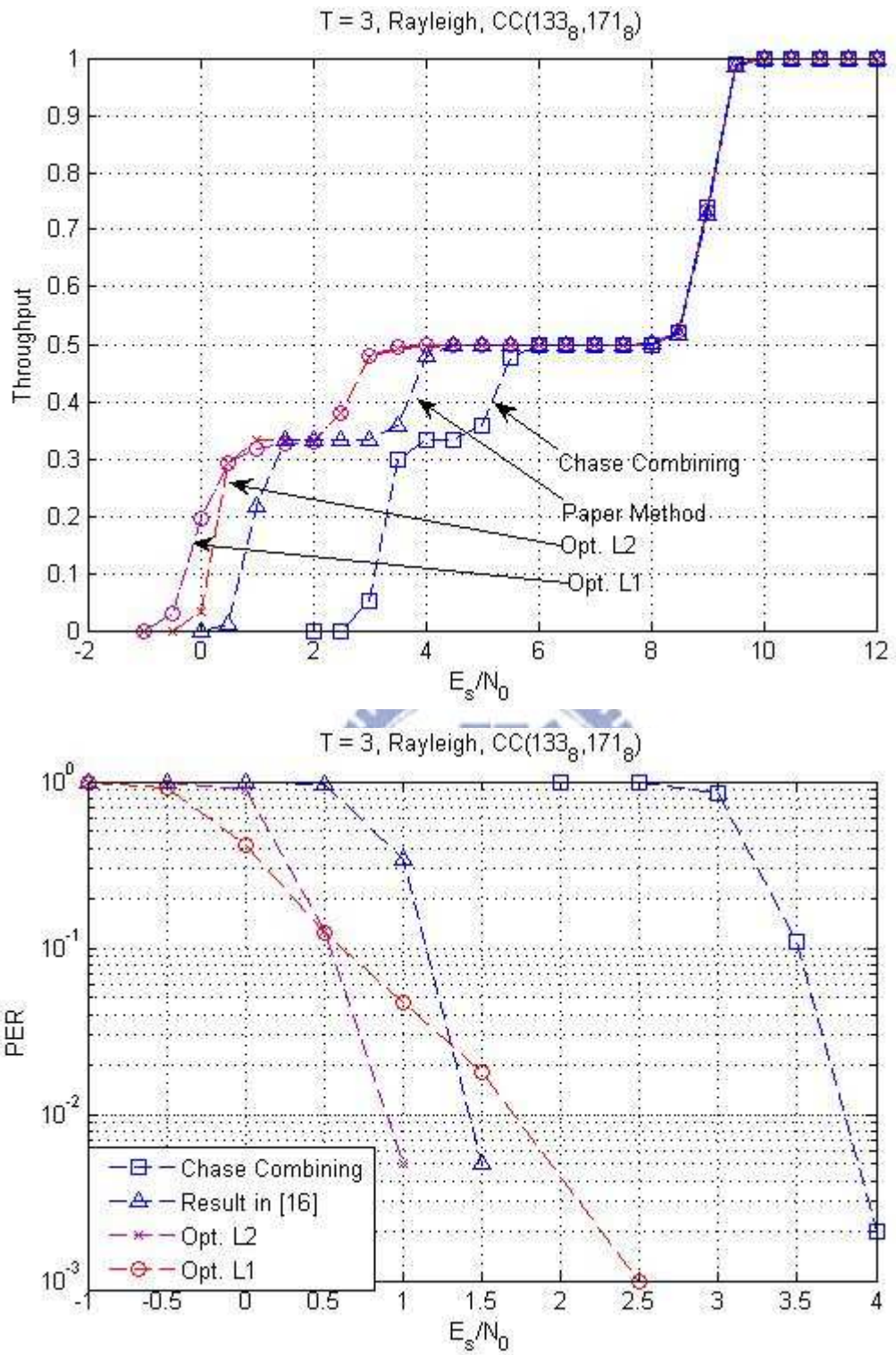


Fig. 5.9 Throughput of the suitable labeling for CC ( 1338 , 1718 ) with 16-QAM under T = 3

### 5.3.2 CC (133<sub>8</sub>,171<sub>8</sub>) , 8PSK, Rayleigh channel

In the section, the results of 8-PSK for CC (133<sub>8</sub> , 171<sub>8</sub>) under Rayleigh fading channel are given. Fig. 5.9 shows the throughput with  $T = 2$  and  $T = 3$ . It is clear that the performance of our design has about 2 dB gain over the chase combining. Table 5.4 shows the strategy of link adaptation for CC (133<sub>8</sub> , 171<sub>8</sub>) with 8-PSK.

$\backslash \mathbf{s}$	0	1	2	3	4	5	6	7
$\mu_1(\mathbf{s})$	0	2	3	7	4	1	6	5
$\mu_{2,1}(\mathbf{s})$	7	0	3	2	6	5	4	1
$\mu_{2,2}(\mathbf{s})$	7	2	6	3	2	4	5	0
$\mu_{3,1}(\mathbf{s})$	7	2	4	0	5	1	6	3

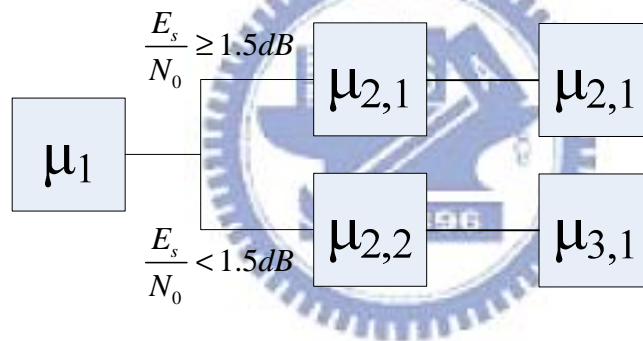


Table 5.4 Strategy of link adaptation for CC (133<sub>8</sub> , 171<sub>8</sub>) with 8-PSK

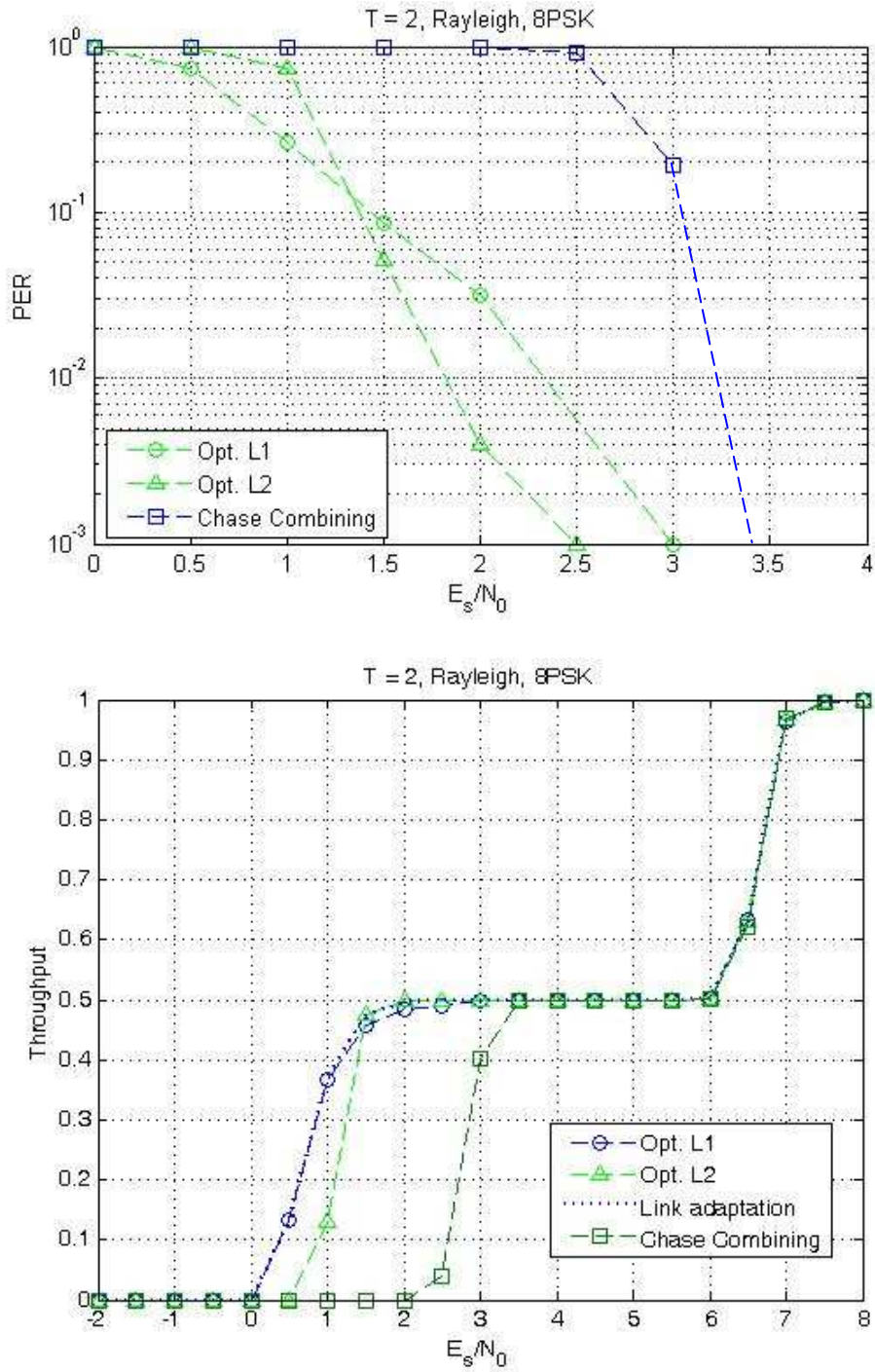


Fig. 5.10 Throughput and PER of the suitable labeling for CC  $(133_8, 171_8)$  with 8-PSK under  $T = 2$



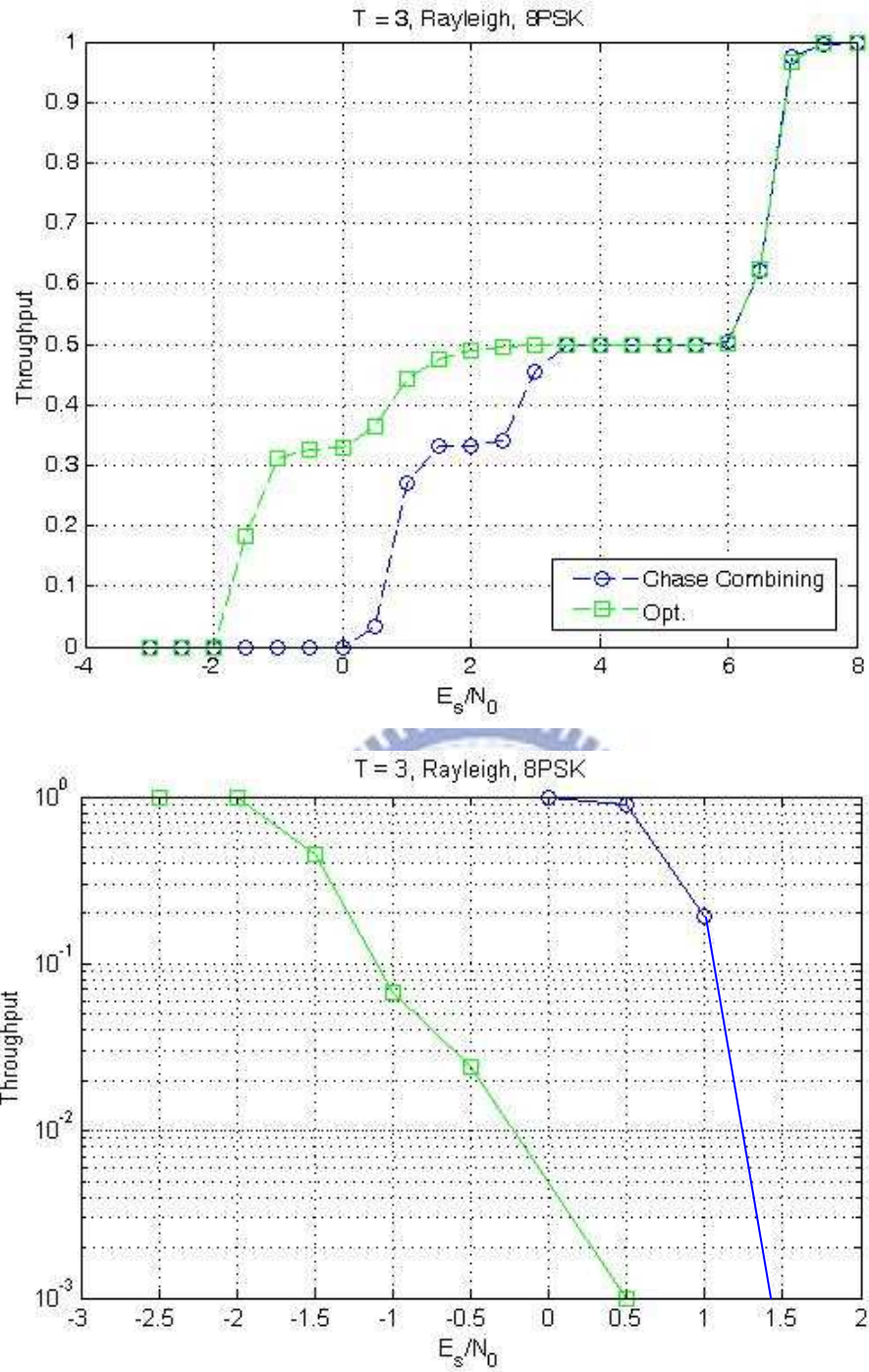


Fig. 5.11 Throughput and PER of the suitable labeling for CC (133<sub>8</sub>, 171<sub>8</sub>) with 8-PSK with 8-PSK under  $T = 3$

## Chapter 6 : Design for 3GPP Turbo Code

In 3GPP HSDPA, a powerful error correction code, turbo code [17], is utilized with HARQ in order to improve the system throughput. In this chapter, a novel HARQ scheme for 3GPP turbo code is proposed. Then, we compare the novel scheme with the existing one from information theoretical point of view. Finally, the Monte Carol simulation results in BER and FER are given to show that the novel decoding scheme has better performance than the conventional one.

### 6.1 HARQ in 3GPP for Turbo Code

In order to further improve the performance of HARQ, a technique named “Constellation rearrangement” is used by 3GPP for turbo code. Constellation rearrangement is a special case of retransmission with different mapping functions, it utilizes different “Gray” code mapping functions (labeling) for retransmissions. [18] shows that constellation rearrangement equalizing the mean bit LLR (reliability) for each bit in multi-level modulation, therefore the performance of HARQ is improved as compared with HARQ using identical Gray labeling.

We can also observe the same result from EXIT chart. Fig. 6.1 shows the transfer curves of constellation rearrangement and conventional chase combining for maximum transmission number equal to 2 and 3. It is obvious that constellation rearrangement performs much better than the conventional chase combining for both  $T = 2$  or 3. The used mapping functions are listed in Table 6.1.

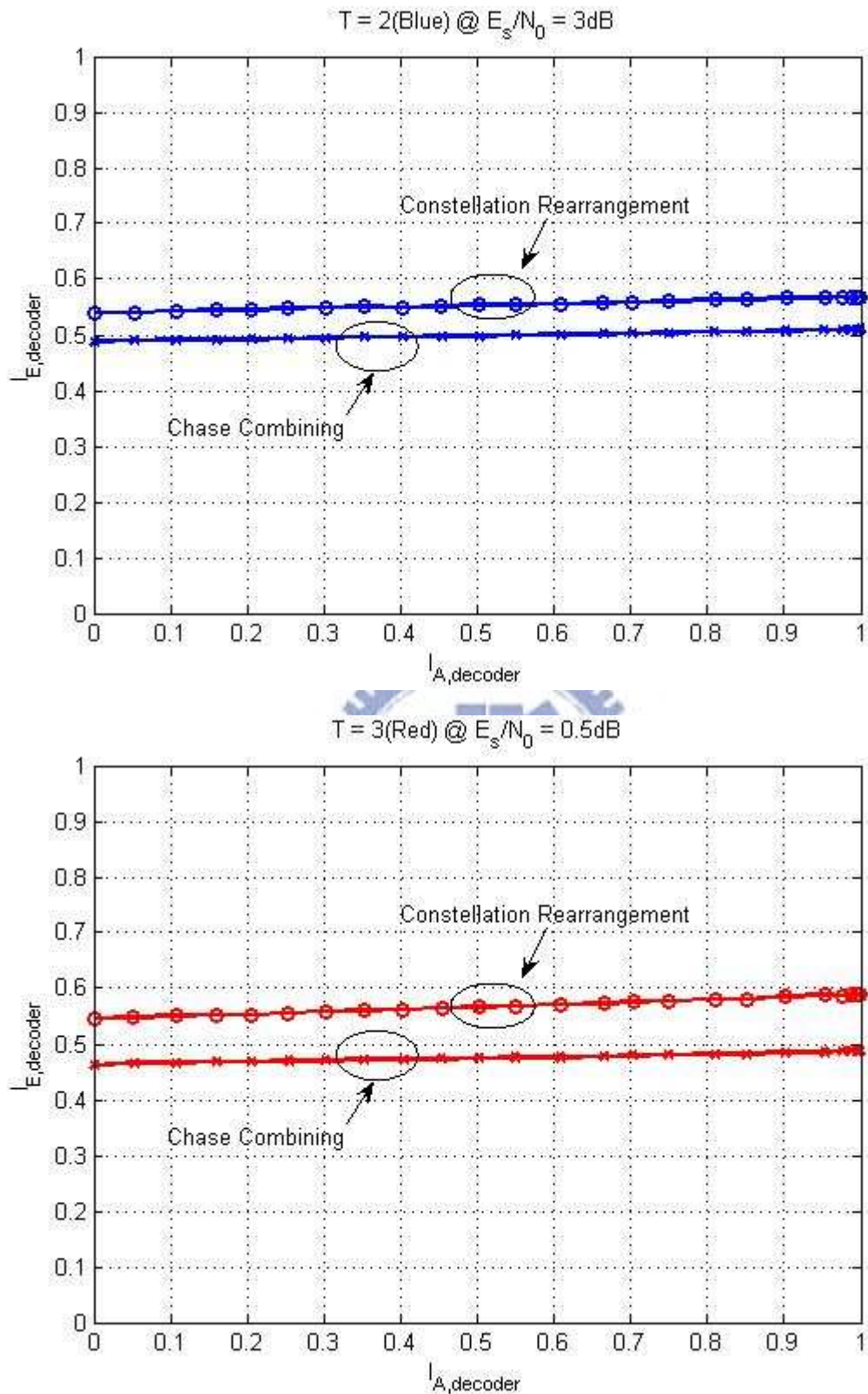


Fig. 6.1 Transfer curves of labeling of chase combining and constellation rearrangement.

$\mu_1 : b_1b_2b_3b_4$	$\mu_2^{ConRr} : \bar{b}_3\bar{b}_4b_1b_2$	$\mu_3^{ConRr} : b_3b_4b_1b_2$
1011 1001	0001 0011	0010 1010
1010 1000	0000 0010	1000 0000
1110 1100	0100 0110	1110 0110
1111 1101	0101 0111	0100 1100
		1010 0010
		0000 1000
		1011 0011
		0001 1001
		1111 0111
		0101 1101

Table 6.1 Mapping functions for constellation rearrangement

## 6.2 Labeling Design for Turbo Code

We fix the mapping function for 1<sup>st</sup> transmission as that used in constellation rearrangement, and then search for a better mapping function for the following retransmissions. Fig. 6.2 shows the results obtained using our algorithm for  $T=2$  or  $T=3$ .

For the case  $T=2$ , It is observed that the new labeling has a similar performance under zero prior condition but performs better with the ideal prior condition. For the case  $T=3$ , although, the new labeling is a little worse than the constellation rearrangement case under zero prior condition, but has much better performance under ideal prior case. Therefore, the new labeling will perform better than the constellation rearrangement.

$\mu_2^{Opt} :$	$\mu_3^{Opt} :$
0011 1111	1010 1011
1011 0111	1111 0100
1101 0001	0010 0011
1001 0101	0000 0110
	0101 0001
	0111 1110
	1000 1001
	1101 1100

\s	0	1	2	3	4	5	6	7	8	9	10	11	12	13	14	15
	10	14	11	15	6	2	7	3	9	13	8	12	5	1	4	0
	5	9	6	10	1	13	2	11	4	8	7	14	0	12	3	15
	2	10	0	12	6	11	5	9	3	15	1	13	7	14	4	8
	2	10	0	12	6	11	5	13	3	15	4	9	7	14	1	8
	7	10	0	12	2	6	5	9	3	15	4	13	11	14	1	8
	0	10	2	12	6	11	5	9	3	15	4	13	7	14	1	8
	14	2	12	5	10	6	9	0	15	7	1	8	3	11	13	4
	7	10	0	12	11	3	5	9	15	2	4	13	6	14	1	8
	2	14	9	5	15	6	12	0	10	7	1	4	3	11	13	8
	2	10	12	5	14	6	9	0	15	7	1	8	3	11	13	4
	2	14	12	5	10	6	0	9	15	7	1	8	3	11	13	4
	12	0	6	14	3	15	9	10	2	5	8	11	4	1	7	13
	2	9	4	15	12	7	10	1	8	3	5	14	6	13	0	11
	2	13	4	15	12	7	10	1	8	3	14	5	6	9	0	11
	2	9	4	15	12	3	10	1	8	7	14	5	6	13	0	11
	0	14	11	5	3	8	13	6	10	4	1	15	12	2	7	9

/s	0	1	2	3	4	5	6	7	8	9	10	11	12	13	14	15
	10	14	15	11	9	13	8	12	6	2	7	3	5	1	4	0
	1	5	2	6	13	9	14	11	4	0	3	7	12	8	15	10
	1	10	2	6	13	9	14	5	4	0	3	7	12	8	15	11
	5	10	13	9	0	14	1	6	15	11	12	8	3	7	2	4
	15	5	3	10	1	7	0	14	9	13	2	6	8	12	4	11
	1	10	2	4	14	6	13	11	9	0	3	7	12	8	15	5
	0	6	14	5	11	2	1	7	13	12	4	15	8	9	3	10
	9	10	2	4	14	8	13	11	6	0	1	7	12	3	15	5
	7	1	14	10	12	11	3	9	13	15	2	5	0	4	8	6
	10	13	0	14	1	15	11	5	12	2	6	8	7	9	4	3
	12	6	4	14	1	15	11	5	7	8	9	2	13	3	0	10

(a)

(b)

Table 6.2 Mapping functions for our design, (a) candidates for second transmission and the optimal one, (b) candidate for third transmission and the optimal one

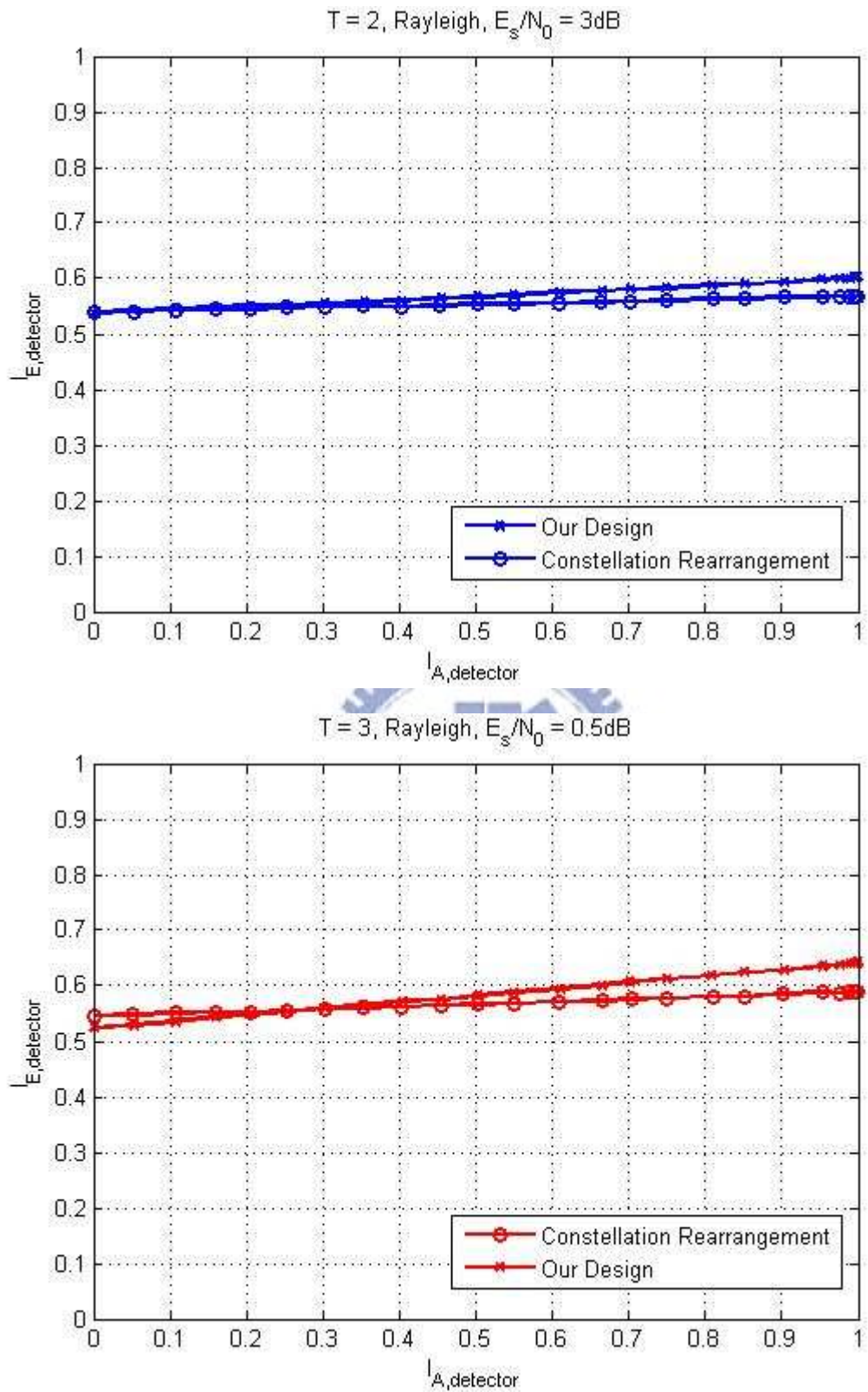


Fig. 6.2 Transfer curves of labeling of chase combining and our design.

## 6.3 Novel Decoder Design for Turbo Code

In the conventional BICM with turbo code, usually the LLR from detector is sent to the decoder that decodes the information using the maximum allowable inner iteration number, that is, no outer iteration is performed. We modify the decoding scheme to take advantage of outer iteration with the constraint on the maximum allowed inner iteration number. The reason is that in a BICM with turbo code system inner iteration is much complicated than outer iteration and the complexity is determined mainly by the number of total inner iterations.

Fig. 6.3 shows the system model of BICM-ID with turbo code. The inner iteration is defined as that between the two BCJR decoders, and the outer iteration is defined as the one between detector and the turbo decoder. As mentioned above, traditionally it performs no outer iteration and executes all allowable inner iteration at once. The extrinsic information from the 2<sup>nd</sup> BCJR decoder is called "*Prior*" of the 1<sup>st</sup> BCJR decoder. We modify the decoding scheme to keep the *prior* of the 1<sup>st</sup> BCJR decoder for the next inner iteration, and perform one inner iteration followed by a outer iteration until the maximum number of inner iteration is reached. Briefly speaking, an inner iteration is followed by a outer iteration with that *Prior* was kept.

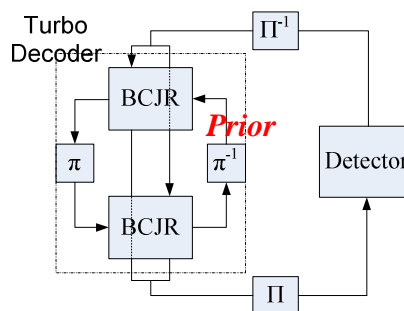


Fig. 6.3 System model of BICM-ID with turbo code

## 6.4 Analysis of Conventional and Modified Decoder

### 6.4.1 Information theoretical point of view

In this section, we compare the conventional scheme and the modified one from the information theoretical point of view. Fig. 6.4 shows a system model of BICM-ID with turbo code, where  $I_i^{DM}(\mathbf{c})$  is the mutual information between the detector extrinsic and coded bits under the  $i$ -th outer iteration, and  $I_i^{DC}(\mathbf{c})$  is the mutual information between the decoder extrinsic and coded bits under  $i$ -th outer iteration.  $I_{i,j}^{DC^k}(\mathbf{b})$  is the mutual information between information bits and extrinsic from decoder  $k$  under  $i$ -th outer iteration and  $j$ -th inner iteration. The functionality of detector is modeled as a function  $h$ , that is,  $I_{i+1}^{DM}(\mathbf{c}) = h(I_i^{DC}(\mathbf{c}), \mathbf{Y})$ . The two BCJR decoder are modeled as  $I_{i,j}^{DC1}(\mathbf{c}) = f(I_i^{DC}(\mathbf{c}), I_{i,j-1}^{DC2}(\mathbf{c}))$  and  $I_{i,j}^{DC2}(\mathbf{c}) = f(I_i^{DC}(\mathbf{c}), I_{i,j}^{DC1}(\mathbf{c}))$ .  $I_{i,0}^{DC2}(\mathbf{c})$  is set to zero in the conventional decoding strategy but set to  $I_{i-1,1}^{DC2}(\mathbf{c})$  in our design.  $I_0^{DC}(\mathbf{c})$  is set to zero initially. We suppose that the extrinsic of decoder or detector is not less reliable than the intrinsic of them, that is,  $I_{i+1}^{DM}(\mathbf{c}) \geq I_i^{DC}(\mathbf{c})$ ,  $I_{i,j+1}^{DC1}(\mathbf{b}) \geq I_{i,j}^{DC2}(\mathbf{b})$  and  $I_{i,j}^{DC2}(\mathbf{b}) \geq I_{i,j}^{DC1}(\mathbf{b})$ .



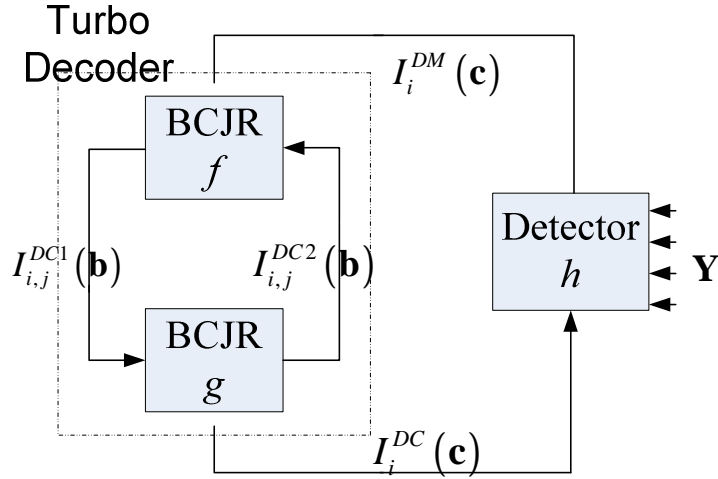


Fig. 6.4 System model of BICM-ID with turbo code

Inner Iteration	Conventional	Modified
Use		
1	$I_1^{DM}(\mathbf{c}) = h(\mathbf{0}, \mathbf{Y})$ $I_{1,1}^{DC1}(\mathbf{b}) = f(I_1^{DM}(\mathbf{c}), \mathbf{0})$ $I_{1,1}^{DC2}(\mathbf{b}) = f(I_1^{DM}(\mathbf{c}), I_{1,1}^{DC1}(\mathbf{b}))$	$I_1^{DM}(\mathbf{c}) = h(\mathbf{0}, \mathbf{Y})$ $I_{1,1}^{DC1}(\mathbf{b}) = f(I_1^{DM}(\mathbf{c}), \mathbf{0})$ $I_{1,1}^{DC2}(\mathbf{b}) = f(I_1^{DM}(\mathbf{c}), I_{1,1}^{DC1}(\mathbf{b}))$
2	$I_{1,2}^{DC1}(\mathbf{b}) = f(I_1^{DM}(\mathbf{c}), I_{1,1}^{DC2}(\mathbf{b}))$ $I_{1,2}^{DC2}(\mathbf{b}) = f(I_1^{DM}(\mathbf{c}), I_{1,2}^{DC1}(\mathbf{b}))$	$I_2^{DM}(\mathbf{c}) = h(I_1^{DC}(\mathbf{c}), \mathbf{Y})$ $I_{2,1}^{DC1}(\mathbf{b}) = f(I_2^{DM}(\mathbf{c}), I_{1,1}^{DC2}(\mathbf{b}))$ $I_{2,1}^{DC2}(\mathbf{b}) = f(I_2^{DM}(\mathbf{c}), I_{2,1}^{DC1}(\mathbf{b}))$
	⋮	⋮

Table 6.3 Analysis in information theoretically point of view for conventional scheme and modified scheme

Table 6.2 shows the change of mutual information between iterative decoding. It is separate by the number of inner iteration. During 1<sup>st</sup> inner iteration, it can be observed that  $I_{1,1}^{DC1}(\mathbf{b})$  and  $I_{1,1}^{DC2}(\mathbf{b})$  in conventional scheme and modified scheme are similar because  $I_1^{DM}(\mathbf{c})$  in both scheme are similar if the leftest point on EXIT chart of labelings in both scheme are almost the same. During 2<sup>nd</sup> inner iteration, the input from detector has been updated by turbo decoder

extrinsic and received channel symbols in our design, that is,  $I_2^{DM}(\mathbf{c}) = h(I_1^{DC}(\mathbf{c}), \mathbf{Y})$  but unchanged in conventional scheme. Therefore,  $I_{1,2}^{DC1}(\mathbf{b})$  in conventional scheme is less reliable than  $I_{2,1}^{DC1}(\mathbf{b})$  in our design since  $I_{2,1}^{DC1}(\mathbf{b})$  is generate by reliable intrinsic from detector, that is,  $I_2^{DM}(\mathbf{c}) \geq I_2^{DM}(\mathbf{c})$ , accordingly  $I_{2,1}^{DC2}(\mathbf{b})$  is more reliable than  $I_{1,2}^{DC2}(\mathbf{b})$  as well.

In terms of the observations above, it is shown that the mutual information between decoder extrinsic and information bit in our design is much reliable than that in conventional decoding scheme under identical inner iteration number.

## 6.4.2 Numeric Values

The simulation environment is listed as in Table 6.4

	Conventional	Modified
# of inner iteration	8	8
Code Rate	$\frac{1}{2}$	$\frac{1}{2}$
BCJR Decoder	max-log	max-log
Detector	MAP	MAP
Labeling	constellation rearrangement	Our Design
# of information bits per packet	5000	5000

Table 6.4 Simulation parameter for 3GPP turbo code

Fig. 6.5 and Fig. 6.6 show the mutual information between decoder extrinsic and information bits of 1<sup>st</sup> and 2<sup>nd</sup> BCJR decoders versus inner iteration number. First, to fix the decoding scheme, we can observe that the extrinsic of each decoder is more and more reliable when inner iteration number increase, and the extrinsic of decoder is more reliable than it's intrinsic. If we focus on Fig. 6.5 and Fig. 6.6

individually, it is obvious that the extrinsic of our design is much reliable than which of conventional design under identical inner iteration number. These results match the theoretical analysis in previous section.

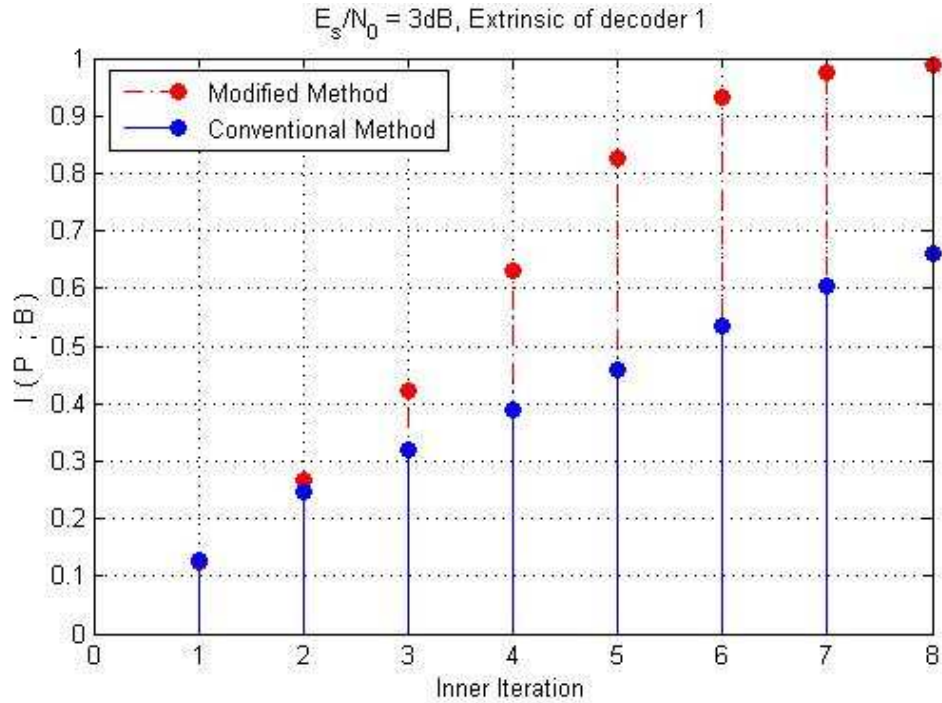


Fig. 6.5 Mutual information between information bit and 1<sup>st</sup> decoder extrinsic

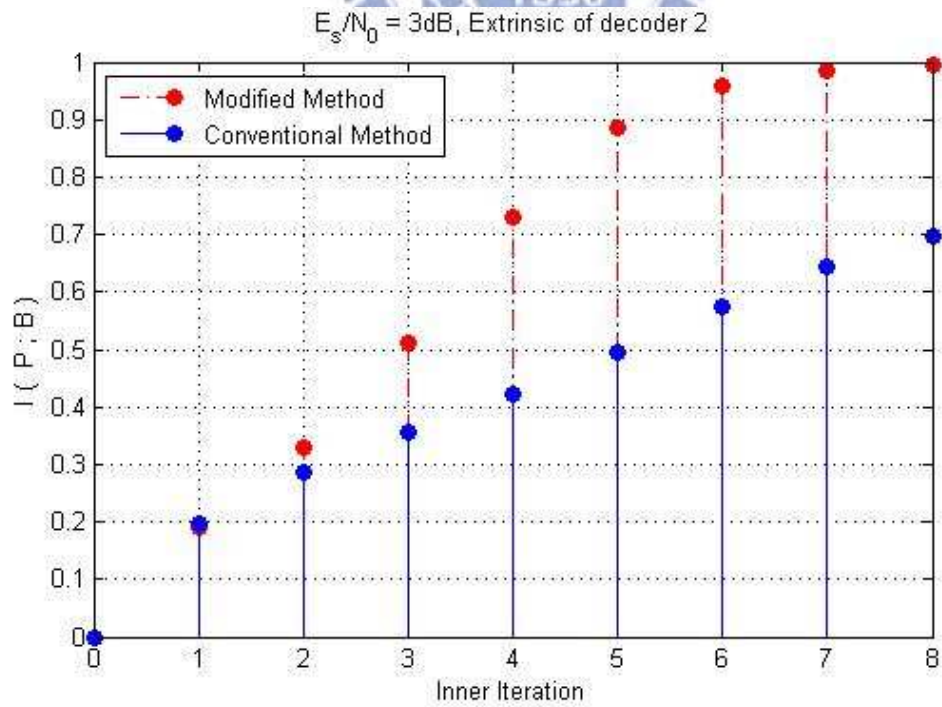


Fig. 6.6 Mutual information between information bit and 2<sup>nd</sup> decoder extrinsic

More precise behavior of our design can be observed in Fig. 6.7. The trajectory is shown in Fig. 6.7, and the decoder transfer curves are plotted with distinct mutual information between prior and information bits, that is,  $I(P;B)$  equal to 0,0.1, ...,0.9. Base on mutual information between prior and information bits shown in Fig. 6.6, the trajectory matches the detector transfer curve and decoder curves perfectly, ex: in the first outer iteration, the decoder transfer with  $I(P;B)$  equal to 0 is matched and in the second outer iteration, the decoder transfer with  $I(P;B)$  equal to about 0.2 is matched and so on.

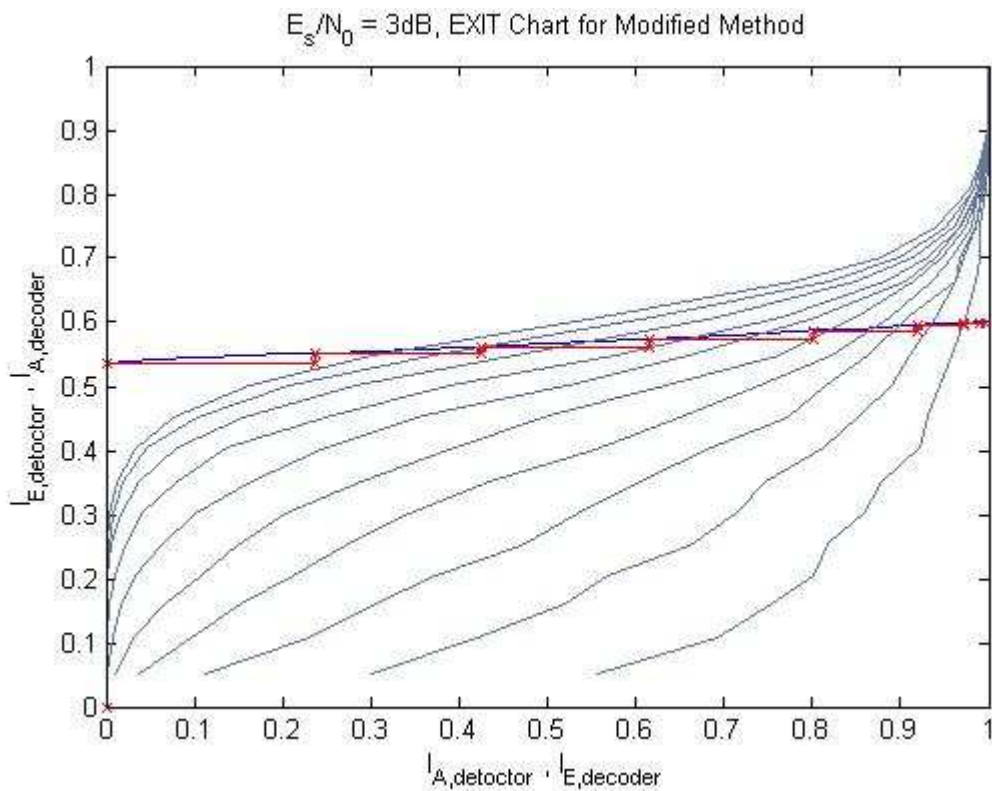


Fig. 6.7 Trajectory of iterative decoding in our design

## 6.5 Simulation Results

In this section, we compare the BER, PER and throughput for conventional scheme and modified scheme under  $T = 2$  and 3. The performance of BER and

PER are plotted on Fig. 6.8 and Fig. 6.9, and we can observe that our design have gains about 0.4dB in case  $T = 2$  and 0.25dB in case  $T = 3$  as compared with constellation rearrangement, and Fig. 6.10 shows throughput performance, our design have gains about 0.4dB in case  $T = 2$  and in case  $T = 3$ .

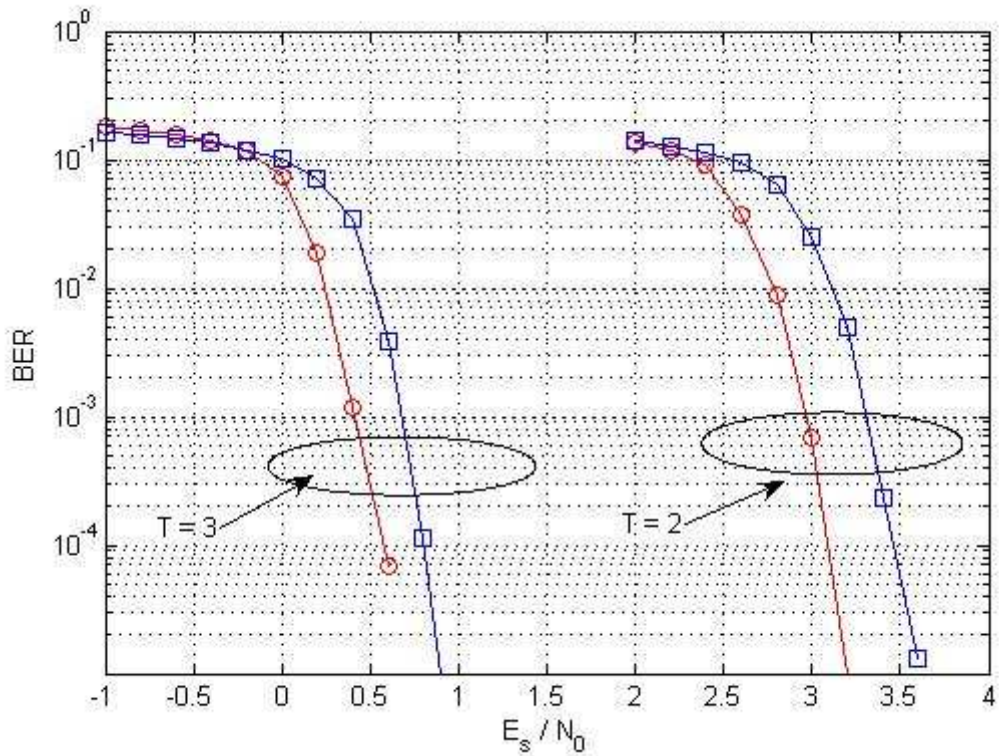


Fig. 6.8 BER of constellation rearrangement ( $\square$ ) and our design ( $\circ$ )

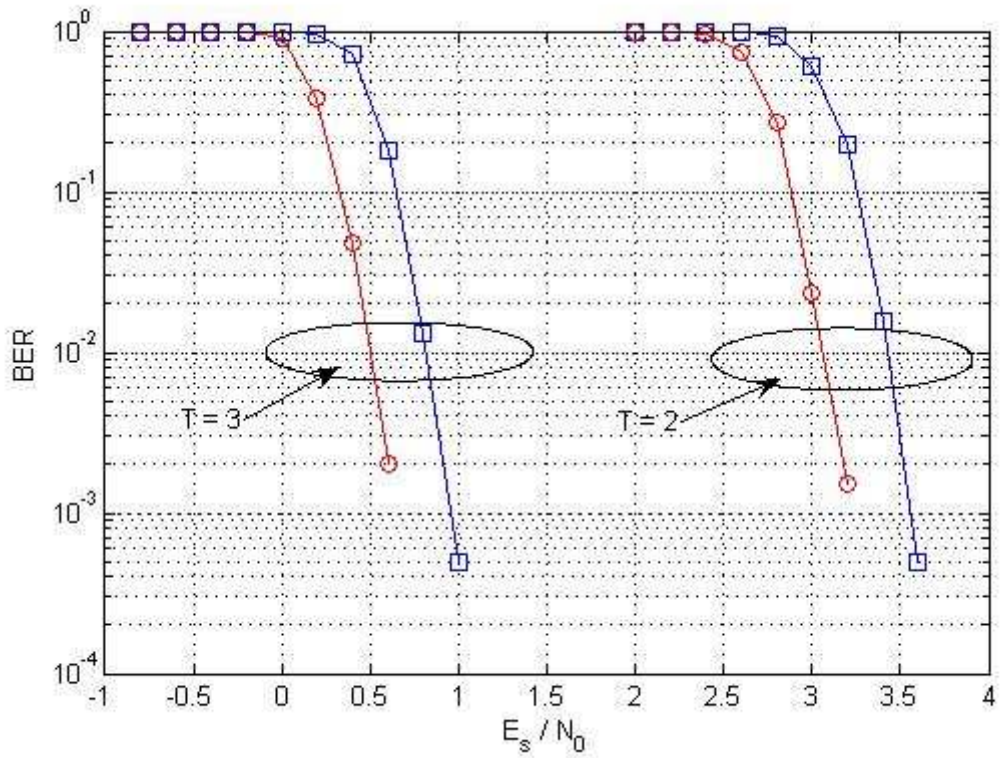


Fig. 6.9 PER of constellation rearrangement (□) and our design (○)

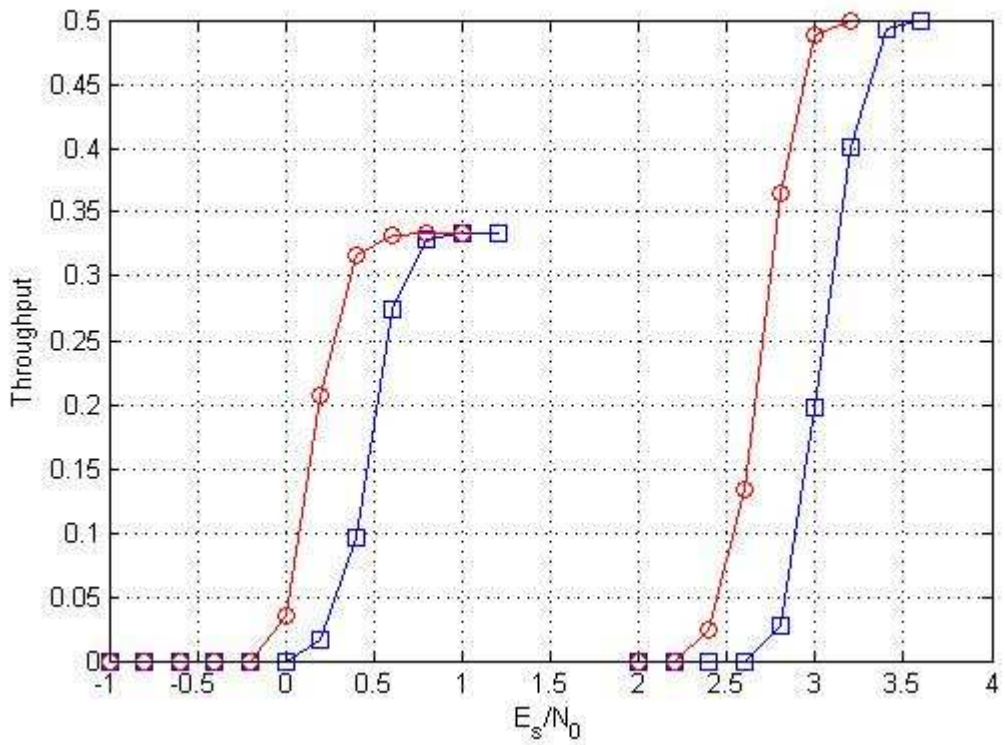


Fig. 6.10 Throughput of constellation rearrangement (□) and our design (○)

## Chapter 7 : Conclusions

In this thesis, we developed a systematic algorithm to search for good labeling used for retransmissions in the Type-I HARQ systems for BICM-ID systems. Link adaptation with different labeling for retransmission is proposed with 2-3 dB performance improvement over the traditional chase combining scheme.. We also consider the novel HARQ scheme used in 3GPP HSDPA. The performance of our design has a gain of about 0.3~0.4 dB as compared with the design in 3GPP [18].



## Reference

- [1] G. Ungerboeck, "Channel coding with multilevel phase signals," *IEEE Trans. Inform. Theory*. vol.IT-28, pp.56-67, Jan 1982.
- [2] G. Caire, G. Taricco and F. Biglieri, "Bit-interleaved coded modulation," *IEEE Trans. Inform. Theory*. vol. 44, no. 3, May 1998.
- [3] E. Zehavi, "8-PSK trellis codes for a Rayleigh channel," *IEEE Trans. Commun.*, vol. 40, pp. 873-884, May 1992.
- [4] X. Li and J. A. Ritcey, "Bit-interleaved coded modulation with iterative decoding," *IEEE Commun. Lett.*, vol. 1, pp. 169-171, Nov. 1997.
- [5] 3GPP (Third Generation Partnership Project) Tech. Specs. [Online]. Available : <http://www.3gpp.org>
- [6] "Air Interface for Fixed and Mobile Broadband Wireless Access Systems," IEEE Std 802.16e-2005.
- [7] D. Chase, "A combined coding and modulation approach for communications over dispersive channels," *IEEE Trans. Commun.*, vol. COM-21, no. 3, pp. 159–174, Mar. 1973.
- [8] D. M. Mandelbaum, "Adaptive-feedback coding scheme using incremental redundancy," *IEEE Trans. Inform. Theory*, vol. IT-20, no. 3, pp. 388–389, May 1974.
- [9] S. ten Brink, "Convergence behavior of iteratively decoded parallel concatenated codes," *IEEE Trans. Commun.* vol. 49, no. 10, Oct. 2001.
- [10] T. W. Yu, C. Y. Wang, C. H. Wang, and W. H. Sheen, "EXIT-Chart Based Labeling Design for Bit-interleaved Coded Modulation with Iterative Decoding," *IEEE ISIT. Proc.*, Dec. 2007.



- [11] Ch. Wengerter, A. Golitschek Edler von Elbwart, E. Seidel, G. Velev, M.P. Schmitt," *Advanced Hybrid ARQ Technique Employing a Signal Constellation Rearrangement*," *IEEE VTC. Proc.*, vol. 4, Fall 2002.
- [12] S. Lin and D. J. Costello, Jr., "*Error Control Coding*". Pearson Prentice Hall, 2003.
- [13] D. Divsalar and F. Pollara, "*Turbo codes for PCS applications*," *IEEE Int. Conf. Proc. Communications*, vol. 1, pp. 54–59. , Jun. 1995
- [14] L. R. Bahl, J. Cockes, F. Jelinek, and J. Raviv," *Optimal Decoding of Linear Codes for Minimizing Symbol Error Rate*," *IEEE Trans. Inform. Theory*, IT-20:284-87, March 1974.
- [15] Qi, X.; Zhou, S.; Zhao, M.; Wang, J., "*Design of constellation labelling maps for iteratively demapped modulation schemes based on the assumption of hard-decision virtual channels*," *Communications, IEE Proc.*, vol.152, no.6, pp. 1139-1148, 9 Dec. 2005
- [16] J. Roberson, Z. Ding, "*A BICM approach to Type-II Hybrid ARQ*," *IEEE ASSP. Conf. Proc.* vol.4, May 2006
- [17] Berrou, C.; Glavieux, A.; Thitimajshima, P., "*Near Shannon limit error-correcting coding and decoding: Turbo-codes*," *IEEE Communications conf.*, vol.2, no., pp.1064-1070 vol.2, 23-26 May 1993
- [18] Wengerter, C.; von Elbwart, A.G.E.; Seidel, E.; Velev, G.; Schmitt, M.P., "*Advanced hybrid ARQ technique employing a signal constellation rearrangement*," *IEEE VT. Conf. Proc.* vol.4, no., pp. 2002-2006, 2002